AD-A124 803 HEAT TRANSFER/BOUNDARY LAYER INVESTIGATION OF HEATING DISCREPANCIES IN WI..(U) AIR FORCE INST OF TECH WRIGHT-PATTERSON AFB OH SCHOOL OF ENGI.. P T CAPPELANO

UNCLASSIFIED DEC 82 AFIT/GA/AA/82D-3 F/G 20/13 NL

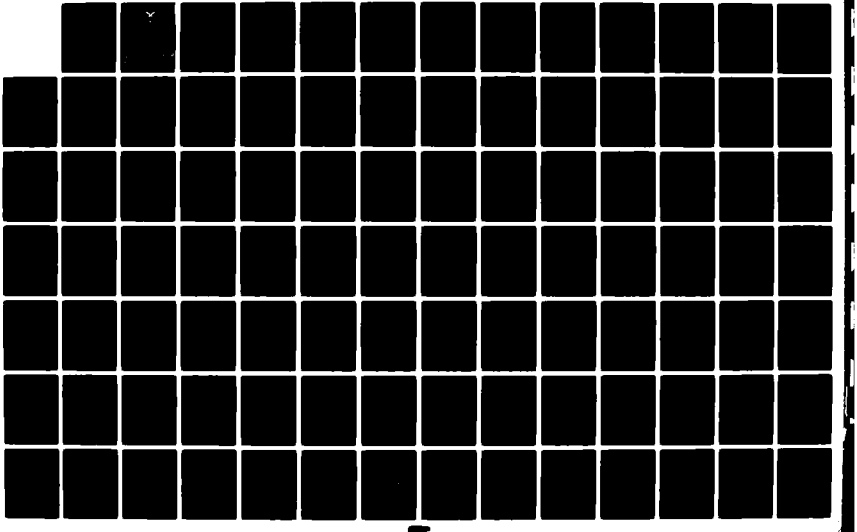

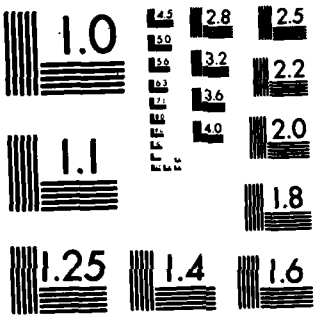

DEPARTMENT OF THE AIR FORCE

AIR UNIVERSITY (ATC)

AIR FORCE INSTITUTE OF TECHNOLOGY

Wright-Patterson Air Force Base, Ohio

AFIT/GA/AA/82D-3

HEAT TRANSFER/BOUNDARY LAYER INVESTIGATION OF HEATING DISCREPANCIES IN WIND TUNNEL TESTING OF ORBITER INSULATING ARTICLES

THESIS

AFIT/GA/AA/82D-3 Peter T. Cappelano
2d Lt USAF

Approved for public release; distribution unlimited

AFIT/GA/AA/82D-3

HEAT TRANSFER/BOUNDARY LAYER INVESTIGATION OF HEATING DISCREPANCIES IN WIND TUNNEL TESTING OF ORBITER INSULATING ARTICLES

THESIS

Presented to the Faculty of the School of Engineering
of the Air Force Institute of Technology
Air University
in Partial Fulfillment of the
Requirements for the Degree of
Master of Science

by

Peter T. Cappelano, B.S.
2nd Lt USAF
Graduate Astronautical Engineering

December 1982

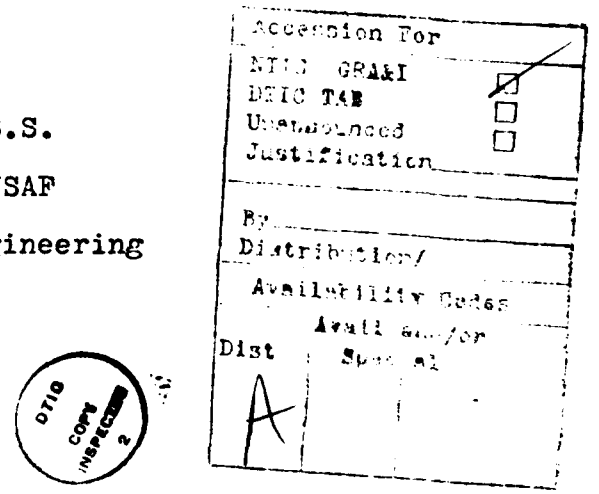

Preface

The success of the Space Shuttle Transportation System will have a great deal of influence on this nation's policy and attitude toward space. Since the U.S. Air Force has been given charge of military operations of the Space Shuttle, opportunities in terms of operations and support for this versatile system are increasing in the military. I am personally very interested in being a part of this new mission of the Air Force. Because of my great personal interest and desire to learn more of the Shuttle's capabilities, I welcomed any opportunity to involve my thesis work in a related subject, with an adviser well informed on Space Shuttle operations. I was extremely fortunate when Capt James K. Hodge was assigned to the faculty here at AFIT. With him came the chance to learn much more of the Space Shuttle system and of flight into and from the space environment.

The completion of this project would not have been possible without the guidance, support, and tolerance of a number of people. The effort I put forth would have been futile without the constant guidance and supervision of Capt Hodge, who, as my adviser, steered me through many obstacles and delays, and led me to the results found here. In addition, Dr. Wilbur Hankey was very helpful in directing me to resources and in raising questions that could only be posed through experience. I want to also thank Dr. James Hitchcock for being available to me at all times and providing addition-

al methods to me. Dr. Joe Shang and Mr. George Havener also deserve thanks for the computer program used in this investigation. Lastly, I want to especially thank my wife Lisette for patience and support as I fretted my way through this project, and for her help in preparing this report.

Peter T. Cappelano

Contents

List of Figures

List of Tables

List of Symbols

α	Deflection angle of experimental plate
c_p	Specific heat capacity at constant pressure
Δ	Small change or increment
γ	Specific heat ratio
h	Heat transfer coefficient
h_{ref}	Reference heat transfer coefficient
h_x	Local heat transfer coefficient
k	Conductivity
L	Total plate length
μ	Viscosity
μ_e	Boundary layer edge viscosity
μ_∞	Freestream viscosity
Nu_x	Local Nusselt Number
Pr	Prandtl Number
$\dot{q}''_o$	Heat flux at surface, Superposition analysis
r	Recovery factor
Re_x	Local Reynolds Number
ρ	Density
ρ_e	Fluid density at boundary layer edge
ρ_∞	Fluid density in freestream flow
St_x	Local Stanton Number
T	Temperature
T_e	Boundary layer edge temperature
T_r	Recovery temperature
T_w	Wall or surface temperature

T_{w1}	Initial wall temperature
T_{w2}	Wall temperature after step
T_o	Surface temperature, Superposition analysis
T_∞	Freestream temperature
T^*	Reference temperature defined by Eckert
θ	Dimensionless temperature potential, Superposition analysis
θ_y	Variation of temperature potential in the direction normal to the surface
u	Velocity
u_e	Velocity at the boundary layer edge
u_∞	Freestream velocity
x	Streamwise location along surface
ξ	Unheated plate length, Superposition analysis
ξ_i	Unheated length for temperature discontinuity T_i
y	Location in the direction normal to the surface

Abstract

Wind tunnel test runs were conducted on Space Shuttle orbiter insulating articles. The data from one HRSI run was processed by a heat estimation program, revealing a large discrepancy in magnitude of the heat transfer coefficient over the HRSI tile when compared to that yielded by flat plate theory and thin skin results. An initial suggestion for the cause of this discrepancy was the nonisothermal wall effect. This effect was the subject of this investigation. The boundary layer heat transfer coefficient was evaluated using a numerical boundary layer program, supplemented by wall temperature superposition analysis. The program was shown to give results consistent with Eckert high speed, flat plate theory for the isothermal wall. A comparison of Sutherland's Law and a low temperature viscosity calculation showed little difference for the high speed flow. Theory based on reference temperature supported this result. The program was modified for wall temperature step over the insulating article to model heat transfer coefficient dependence on wall temperature variation. The step size was varied by doubling and quadrupling the initial step size, and by doubling the initial wall temperature. The magnitude of the heat transfer coefficient decreased, and response slowed, with increasing step size. The step location was also varied. Analysis by wall temperature superposition yielded results similar to program results with the initial wall temperature step. The nonisothermal wall

effect appears to account for most of the discrepancy in the original wind tunnel test results.

HEAT TRANSFER/BOUNDARY LAYER INVESTIGATION OF HEATING DISCREPANCIES IN WIND TUNNEL TESTING OF ORBITER INSULATING ARTICLES

I. Introduction

Background

The successful introduction of the Space Shuttle system into service marks the beginning of a new era in the utilization of the space environment. A manned vehicle capable of entry into space and controlled, gliding reentry with the additional quality of reusability is a great step toward increased affordability and reliability in terms of space transportation. Repeated use translates directly into reduced cost to travel into space. Controlled, gliding reentry means greater versatility in selection of landing sites and reentry points. These two qualities separate the Space Transportation System (STS) from previous modes of space travel. These qualities also place greater emphasis on the capability of the Orbiter Thermal Protection System (TPS) in the reentry heating environment (Ref 1:2). Reusability requires that the TPS be able to sustain reentry heating repeatedly. Gliding entry requires that the TPS be able to sustain reentry heating through a variety of maneuvers and attitudes. Consequently, the capability of the Thermal Protection System must be thoroughly understood through testing and evaluation.

The Air Force Flight Test Center (AFFTC) has been conducting this evaluation through aerothermodynamic performance simulation, and collection and reduction of in-flight thermocouple data from the Reusable Surface Insulation (RSI) on the Orbiter. The data reduction was accomplished using a computer code to extract aerodynamic heat rate and TPS parameters from transient flight test maneuvers. This program is referred to as HEAT ESTimation or HEATEST. In addition to data from actual Shuttle flights, thermocouple measurements from Mach 14 wind tunnel tests with TPS articles were obtained and reduced (Ref 1:2).

Problem Statement

The wind tunnel testing was conducted by the Air Force Wright Aeronautical Laboratories (AFWAL) in a circular cross-section, Mach 14 wind tunnel. Tests were made using three different type articles: a thin skin stainless steel plate, a High-temperature Reusable Surface Insulation tile (HRSI), and a Flexible Reusable Surface Insulation tile (FRSI). The test articles were flush mounted on a test plate with a wedge-shaped leading edge. Thermocouple measurements were taken at several streamwise locations for each article, as indicated in Figs 1, 2, and 3. A total of 59 test runs were catalogued. Runs 1-26 were conducted with an HRSI tile. During these runs, the deflection angle of the test plate was varied. This served two purposes. First, the angle could be made large to induce faster heating response and subsequently lowered in order to achieve heating equilibrium on the test article. This would

reveal a limiting temperature for given conditions. Second, variation of the deflection angle could simulate flight maneuvers and give some indication of transient heating response. The actual sequences used are given in Table I. In addition, Runs 27-45 were conducted with an FRSI test article and Runs 46-59 were conducted with a thin skin article. The sequences for these are given in Tables II and III, respectively. As indicated in some cases, a shock generator was used to simulate shock interaction. Also, in the HRSI and FRSI test runs, a water cooled plate parallel to the test articles was used to maintain a somewhat reliable radiation sink temperature (Ref 1:8).

Wind tunnel data for test run 4, with an HRSI test article, was input to the analysis program, HEATEST, to extract heat transfer data. The sequence of variation of the deflection angle for this run and the associated temperature-time history are given in Fig 4. The plate was injected at α = 14 degrees and held for approximately ten seconds, allowing rapid temperature response. The deflection angle was then lowered to α = 3 degrees and the temperature appeared to level out, indicating that thermal equilibrium was achieved at this deflection angle. Finally, the plate was returned to α = 14 degrees and the temperature climbed for the remainder of the run. The test indicated that equilibrium was achieved at α = 3 degrees .

The data analysis accomplished using HEATEST is given in Fig 5. In this figure, the indicated results reduced through

HEATEST differ markedly from Eckert flat plate theory and thin skin results. At the deflection angle $\alpha = 3$ degrees, theory indicates that the expected value of the heating ratio should be $h/h_{ref} = 1.7$. The HEATEST data indicates the value to be $h/h_{ref} = 0.95$. Additionally, an equilibrium heat rate calculation assuming a radiation sink temperature of $T = 0$ R agrees with the HEATEST value. The same calculation assuming a sink temperature of $T = 533$ R gives a value of h/h_{ref} lower than that derived from HEATEST (Ref 1:9).

From this data, the reliability of the wind tunnel tests is questioned. A discrepancy is seen between HRSI data results and Eckert theory. Thin skin test data seem to agree with theory, indicating an effect only in the HRSI case. Therefore, the primary causes indicated are those differences between thin skin and HRSI materials. The HRSI material has thermal properties quite different from the thin skin stainless steel. Due to extremely low conductivity, the HRSI tile surface temperature should increase much more rapidly than the stainless steel. At a given angle and time, the HRSI tile should be much hotter than the stainless steel surface upstream. The result is a discontinuity in temperature from the steel plate to the HRSI tile. This is the nonisothermal wall problem. Additionally, the HRSI tile achieves equilibrium because it has high emissivity. The stainless steel does not. A valid estimate of the radiation sink temperature is essential to the accuracy of the equilibrium heating calculation. Although a parallel plate of known temperature is

used as a sink, the tunnel wall temperature is unknown and must be considered as a sink for radiation, based on view factor. Additional causes of error that must be considered include inaccuracy in data reduction, inaccuracy in thermocouple data, and variation in the boundary layer and surface heating ahead of the test articles where no data was taken.

Objectives and Approach

In order to make the wind tunnel test data valid and usable, it must be corrected to account for the possible inaccuracies cited. The greatest effects expected are those due to the nonisothermal wall problem, and those caused by misunderstood radiation effects. Without knowledge of the tunnel wall temperature, the radiation cannot be accurately estimated. This precludes pursuing a thorough investigation of thermal radiation and, by equilibrium analysis, derivation of heating data on the test article. By necessity, the focus of this investigation will be the nonisothermal wall effect, and the resultant change in heating attributed to it. Through this investigation, the portion of the discrepancy due to the nonisothermal wall alone may be determined. Additionally, attributing the discrepancy cited to causes unique to the wind tunnel should render greater validity to theoretical estimation of HRSI heating. Knowing the effect of the nonisothermal wall would allow for some estimation of the combined effects of the other sources cited. Finally, the effects of the nonisothermal wall condition can be related to numerous

applications, including the Space Shuttle Orbiter. Several applications will be discussed.

Analysis of the nonisothermal wall effect will require understanding of the boundary layer development, and the effects of heating on boundary layer growth. This analysis will best be accomplished through boundary layer solution techniques. The three methods of solution considered here are: (1) boundary layer similarity, (2) solution of the boundary layer equations by finite-difference technique in a boundary layer program, and (3) wall temperature superposition analysis. The similarity solution of the boundary layer was found to be invalid, as discussed in Appendix A. The results of the boundary layer program and wall temperature superposition method are presented subsequently. The boundary layer program is discussed in Appendix B.

II. Theory

Eckert-Flat Plate Theory

Heat transfer over a flat plate can be calculated simply by Eckert theory based on several assumptions. It is assumed that the flow medium is an ideal, single component gas, with no dissociation. The flow over the plate is assumed to have locally uniform velocity and direction. The boundary layer is assumed thin enough that pressure is transmitted without change to the surface. Surface temperature is assumed constant. Also, the fluid is assumed to have constant properties, independent of temperature and pressure. The following dimensionless quantities are defined as

$$Nu_x = \frac{h_x x}{k} \tag{1}$$

$$St_x = \frac{h_x}{\rho_e c_p u_e} \tag{2}$$

where h_x is the heat transfer coefficient, k is conductivity, ρ is density of the fluid, c_p is the specific heat at constant pressure, and u_e is the velocity of the fluid at the edge of the boundary layer. Nu_x is the local Nusselt Number and St_x is the local Stanton Number. For laminar flow over the plate, the following relations define the temperature recovery factor r, the Nusselt Number, and the Stanton Number:

$$r = \sqrt{Pr} \tag{3}$$

$$Nu_x = 0.332\ Pr^{\frac{1}{3}} Re_x^{\frac{1}{2}} \quad (4)$$

$$St_x = \frac{Nu_x}{Pr\ Re_x} = \frac{0.332}{Pr^{\frac{2}{3}} Re_x^{\frac{1}{2}}} \quad (5)$$

where Pr is Prandtl Number and Re_x is local Reynolds Number defined by

$$Re_x = \frac{\rho_e u_e x}{\mu_e} \quad (6)$$

Note that μ is fluid viscosity and the subscript e denotes boundary layer edge conditions.

For real gases at high velocity and temperature, the properties do vary with temperature. They may be assumed independent of pressure as long as excessively high pressure and dissociation are avoided. Under these circumstances, and as long as c_p can be assumed constant, the preceding relations describing heat transfer can still be used with good accuracy when the fluid properties are calculated at a reference temperature T^*, defined as

$$T^* = T_e + 0.5(T_w - T_e) + 0.22(T_r - T_e) \quad (7)$$

by Eckert (Ref 2:10-13).

The above equations may be used to solve for the heat transfer coefficient. From the Nusselt Number,

$$h_x = 0.332\ Pr^{1/3} Re_x^{1/2} k/x \quad (8)$$

Using the definition of Prandtl Number as

$$Pr = c_p \mu / k \tag{9}$$

the heat transfer coefficient can be reduced to the expression,

$$h_x = 0.332 \frac{c_p}{Pr^{\frac{2}{3}}} \left[\frac{\rho_e u_e \mu_e}{x} \right]^{\frac{1}{2}} \tag{10}$$

Based on Eq (2), definition of Stanton Number, the same relation for heat transfer coefficient is derived. However, other definitions of Stanton Number are given in various sources, including

$$St_x = \frac{h_x}{\rho c_p u_\infty} \tag{11}$$

and

$$St_x = \frac{h_x}{\rho_\infty c_p u_\infty} \tag{12}$$

In all cases, the subscript infinity, ∞, refers to freestream conditions. Based on these varied definitions of Stanton Number, using ideal gas calculations of fluid properties, several definitions of heat transfer coefficient result. From the Stanton Number of Eq (2),

$$h_x = 0.332 \frac{c_p}{Pr^{2/3}} \left[\frac{\rho_e u_e \mu_e}{x} \right]^{\frac{1}{2}} \tag{10}$$

Using Eq (11) to define Stanton Number,

$$h_x = 0.332 \frac{c_p}{Pr^{2/3}} \left[\frac{\rho_e u_\infty^2 \mu_e}{u_e x} \right]^{\frac{1}{2}} \tag{13}$$

Defining Stanton Number as in Eq (12),

$$h_x = 0.332 \frac{c_p}{Pr^{2/3}} \left[\frac{\rho_\infty^2 u_\infty^2 \mu_e}{\rho_e u_e x} \right]^{\frac{1}{2}} \tag{14}$$

Eqs (10), (13), and (14) may be rewritten for the high speed case by substituting for local density ρ_e and viscosity μ_e with values ρ^* and μ^* calculated according to the reference temperature, T^*, defined by Eckert as in Eq (7). The resulting equations are

$$h_x = 0.332 \frac{c_p}{Pr^{2/3}} \left[\frac{\rho^* u_e \mu^*}{x} \right]^{\frac{1}{2}} \tag{15}$$

$$h_x = 0.332 \frac{c_p}{Pr^{2/3}} \left[\frac{\rho^* u_\infty^2 \mu^*}{u_e x} \right]^{\frac{1}{2}} \tag{16}$$

$$h_x = 0.332 \frac{c_p}{Pr^{2/3}} \left[\frac{\rho_\infty^2 u_\infty^2 \mu^*}{\rho^* u_e x} \right]^{\frac{1}{2}} \tag{17}$$

respectively. In addition, Hayes and Neumann (Ref 3:2) introduce the empirical calculation of the ratio of heat transfer coefficients as

$$\frac{h}{h_{ref}} = \left[\frac{P_e}{P_\infty} \right]^{\frac{1}{2}} \tag{18}$$

The above equations will subsequently be used to evaluate reference conditions.

Method of Superposition

The method of wall temperature superposition can be used to develop heat transfer solutions for boundary layer flow

over a plate with arbitrarily varying surface temperature due to the linearity of the boundary layer energy equation, according to Kays (Ref 4:218-219). Assuming constant velocity flow of a constant property fluid over a flat plate, with laminar flow only, the heat transfer coefficient is given as

$$h(\xi,x) = 0.332 \frac{k}{x} Pr^{1/3} Re_x^{\frac{1}{2}} \left[1 - \left(\frac{\xi}{x}\right)^{3/4}\right]^{-1/3} \tag{19}$$

where ξ is defined as the unheated plate length. Defining $\theta(\xi,x,y)$ as

$$\theta(\xi,x,y) = \frac{T_o - T}{T_o - T_\infty} \tag{20}$$

where T_o is the plate surface temperature, T_∞ is the stream temperature beyond the boundary layer, and T is local temperature, a solution to the boundary layer energy equation with arbitrary surface temperature distribution is given by

$$T - T_\infty = \int_o^x \left[1 - \theta(\xi,x,y)\right] \left(\frac{dT_o}{d\xi}\right) d\xi + \sum_{i=1}^{k} \left[1 - \theta(\xi_i,x,y)\right] \Delta T_{o,i} \tag{21}$$

The heat flux from the wall surface is

$$\dot{q}_o'' = -k \left(\frac{\partial T}{\partial y}\right)_{y=0} \tag{22}$$

Substituting for the differential with Eq (25) yields

$$\dot{q}_o'' = k \left[\int_o^x \theta_y(\xi,x,0) \left(\frac{dT_o}{d\xi}\right) d\xi\right.$$

$$+\sum_{i=1}^{k} \theta_y(\xi_i, x, 0)\Delta T_{o,i} \qquad (23)$$

For the isothermal wall case, with wall temperature unequal to freestream temperature,

$$\dot{q}''_o = k\theta_y(\xi, x, 0)\ (T_o - T_\infty) \qquad (24)$$

By convective heat transfer,

$$\dot{q}''_o = h(T_o - T_\infty) \qquad (25)$$

Solving for the heat flux in terms of heat transfer coefficient and conductivity yields

$$\theta_y(\xi, x, 0) = \frac{h(\xi, x)}{k} \qquad (26)$$

Substituting Eq (26) into Eq (23) gives the heat flux due to an arbitrary wall temperature distribution as

$$\dot{q}''_o = \int_o^x h(\xi, x)\left(\frac{dT_o}{d\xi}\right) d\xi + \sum_{i=1}^{k} h(\xi_i, x)\Delta T_{o,i} \qquad (27)$$

where the heat transfer coefficient is defined by Eq (23) (Ref 5:218-219). The local heat transfer coefficient is derived directly from $\dot{q}''_o$ as

$$h_x = \frac{\dot{q}''_o}{(T_o - T_\infty)} \qquad (28)$$

This method may be adapted for the hypersonic velocity conditions by using the reference temperature defined by Eq (7) to calculate the fluid properties, and by substituting the recovery temperature T_r for the freestream temperature.

Low Temperature Viscosity

The standard relationship used to calculate viscosity is that given by Sutherland's Law:

$$\mu = \frac{2.27 \times 10^{-8} \, T^{3/2}}{T + 198.6} \quad \frac{\text{lb-sec}}{\text{ft}^2} \tag{29}$$

According to Fiore (Ref 5), this may not be valid for hypersonic wind tunnel applications. In hypersonic tunnels, the freestream temperature generally falls in a range between $T = 30$ R and $T = 200$ R, depending upon the ambient temperature of the gas and the design Mach number. As a result, the freestream temperature is outside the demonstrated range of applicability of Sutherland's Law. As an alternative calculation, the viscosity can be defined as

$$\mu = \frac{2.32 \times 10^{-8} \, T^{\frac{1}{2}}}{1 + \left(\frac{220}{T \times 10^{9/T}} \right)} \quad \frac{\text{lb-sec}}{\text{ft}^2} \tag{30}$$

This relationship provides good correlation to experimental data for low temperature flow. In addition, calculations of viscosity for temperatures above $T = 300$ R by this low temperature relationship correspond well with viscosity calculations by Sutherland's Law (Ref 6).

III. Test Data

As indicated in the Introduction, a number of wind tunnel tests were conducted using thin skin stainless steel, HRSI, and FRSI test articles. From these, three runs for HRSI and thin skin materials were chosen to yield data at varied deflection angles. In each case, data was extracted for deflection angles of α = 3, 10, and 14 degrees . The selection of the runs used for each case was based on injection at high deflection angle to promote rapid temperature response, and on length of run at the desired deflection angle. For HRSI material, experimental runs chosen were run 4 for α = 3 degrees , run 20 for α = 10 degrees , and run 19 for α = 14 degrees . For thin skin stainless steel, selected runs were run 58 for α = 3 degrees , run 57 for α = 10 degrees , and run 46 for α = 14 degrees . In addition, data for FRSI material runs was taken from runs 29 and 33 for α = 3 degrees. The test sequence for the HRSI cases is given in Table I, for the FRSI cases in Table II, and for the thin skin stainless steel cases in Table III. For the HRSI runs, a time history of the temperature reading on thermocouple T/C No. 5 is given in Fig 6, with location given in Fig 1. For the FRSI runs, the temperature history is given in Fig 7 for thermocouple T/C No. 4, with location given in Fig 2. For the thin skin runs, the temperature history for thermocouple T/C No. 4 is given in Fig 8, with location given in Fig 3.

The thermocouples were chosen to give temperature history

data at the material surface. Fig 6 reveals that the HRSI test article levels out at a temperature of $T = 705$ R for a deflection angle of $\alpha = 3$ degrees before the angle is raised to $\alpha = 14$ degrees, in run 4. Similar indications are gained from run 20, where $T = 760$ R for $\alpha = 10$ degrees, and from run 19, where $T = 810$ R for $\alpha = 14$ degrees. From these, it would appear that thermal equilibrium is achieved in each case. This equilibrium point gives the maximum wall temperature achieved at the thermocouple location used. A similar equilibrium point is seen in the time history data for FRSI material in run 33, Fig 7. This case shows thermal equilibrium for FRSI material at a deflection angle of $\alpha = 3$ degrees to be $T = 700$ R. For run 29, it appears that equilibrium is approached more gradually and is not achieved before the test run is ended. As a result, FRSI surface heating data were taken from run 33 for comparison.

At the thermal equilibrium points for the HRSI and FRSI materials, data readings were extracted for all thermocouple locations. It was found that the HRSI thermocouple T/C No. 6 was not functioning during any of the runs made, as it maintained a constant temperature reading. The location of this thermocouple is given in Fig 1. As a result, only one surface data point was available for HRSI heating results. For FRSI material, run 33 was used to extract a surface temperature distribution at a deflection angle of $\alpha = 3$ degrees. The temperature readings for each location are given in Fig 9. From this data, the FRSI surface temperature is revealed to

vary by only a few degrees above and below a constant of $T = 690$ R . This is a strong indication of constant temperature over the insulating material. Since the thermal design properties of the HRSI material are similar to those of the FRSI material, the surface temperature of the HRSI material will be assumed constant streamwise, at the value given by HRSI thermocouple T/C No. 5 for each deflection angle.

The thermocouple data for the thin skin temperature distribution at each deflection angle were taken from runs 58, 57, and 46, as indicated earlier. A temperature time history for the thin skin article is given in Fig 8 for these runs. It is seen here that the surface temperature increases throughout the test runs for the thin skin cases. Since no equilibrium was achieved, the surface temperature distribution data were arbitrarily taken at the point of maximum value, near the end of each run. The distribution for deflections of $\alpha = 3$, 10, and 14 degrees are given in Figs 9, 10, and 11, respectively. For each case, the thin skin stainless steel surface temperature gradually decreases with streamwise location. This decline is a very small percentage of the surface temperature itself, so the thin skin surface is assumed isothermal at a median wall temperature. Since no data was available for the wedge surface temperature ahead of the test article location, the initial wall temperature was assigned the thin skin value for the given deflection angle, and was assumed constant.

It should be noted that several underlying assumptions made here did not allow duplication of the test conditions in the numerical calculation. The HRSI thermocouple actually lies beneath the radiative coating on the surface, and may not reflect the actual surface temperature. The coating surface temperature may be somewhat higher. The higher deflection angle readings for the HRSI may not be at equilibrium but may be only approaching that condition. A higher temperature at equilibrium would then be expected. Since the wedge surface temperature is unknown, it may not be at the temperature of the thin skin plate. Indeed, the wedge is a much larger heat sink than the thin skin plate in terms of volume. As such, its surface temperature should not rise as quickly as the thin skin surface temperature, but should probably remain close to the initial ambient temperature of the wedge. A possible indication of this temperature difference between the thin skin and wedge stainless steel surfaces is seen in the heat transfer coefficient data given by Hayes (Ref 8) and displayed in Fig 12. Note that this data reveals that the heat transfer coefficient actually rises to a maximum at the location $x = 9$ in , and then declines. For an isothermal wall, the distribution of local heat transfer coefficient should decrease gradually along this entire length, as indicated in Fig 14, with no rise like that seen in the test data. As a result, some wall temperature discontinuity may be present. Note, however, that this rise in the heat transfer coefficient may also be caused by bowing of the heated thin skin

plate as a result of expansion. Higher heating would be seen on the forward part of the plate, with somewhat lower heating on the aft section for this case as well. Also, constant temperature on the wedge ahead of the test article location was assumed, but could not be verified. Finally, the thin skin readings were taken at their maximum values, which may not correspond to the same time coordinate as the HRSI equilibrium readings. The indication of these differences is that the initial wall temperature should probably be lower than the thin skin values assumed, the final wall temperature may be somewhat higher, and the step size is most likely larger than that taken from the test data.

IV. Reference Conditions

Reference Calculation

In studying the variation of heating on the HRSI, FRSI, and thin skin test articles due to deflection angle and wall temperature variation, boundary layer characteristics become very important. The heat transfer to the surface depends on the thermal transport properties of the boundary layer. The convective heat flux is defined as the product of the temperature potential and the heat transfer coefficient. The temperature potential is the difference between the wall temperature and the freestream temperature for low speed flow, or between the wall temperature and recovery temperature for high speed flow. As such, the temperature potential is independent of boundary layer properties. As a result, boundary layer heat transport dependence on wall temperature variation must be reflected in the heat transfer coefficient distribution.

In order to enhance the comparison of results, and eliminate location dependence of the heat transfer coefficient in the comparison, a reference distribution at zero deflection was required. The reference value at location $x/L = 0.575$ is of particular significance since HRSI data are given for this location. This value was calculated by the varied definitions of heat transfer coefficient according to Eckert flat plate and high speed flat plate theory. At a deflection angle of zero degrees, the boundary layer edge values and freestream values of density, velocity, and viscosity are identical, and

Eqs (10), (13), and (14) yield the same results. The reference heat transfer coefficient calculated by Eckert flat plate theory is $h_{ref} = 1.12 \times 10^{-4}$ Btu/ft^{2}s-R , based on the wind tunnel freestream operating conditions. Prandtl Number is assumed constant at $Pr = 0.72$, and the specific heat is assumed constant at $c_p = 6006$ ft^2/s^{2}R . These values will be assumed constant in all subsequent calculations. According to Eckert high speed flat plate theory, the fluid properties are determined according to the reference temperature defined in Eq (7). At zero degree deflection, Eqs (15), (16), and (17) yield the same result for heat transfer coefficient, $h_{ref} = 1.16 \times 10^{-4}$ Btu/ft^{2}s-R .

As indicated in the Theory section, Sutherland's Viscosity Law may not be valid at low freestream temperatures. An alternate form given by Eq (30) can be used to estimate a reference heat transfer coefficient. The variation between this relationship and that given by Sutherland's Law is negligible above a temperature of $T = 300$ R , as seen in Fig 13. Below $T = 300$ R , there is significant divergence, with the low temperature calculation yielding viscosity values greater than those given by Sutherland's Law at the same temperature. As a result, when applied to Eq (10), the low temperature calculation reveals a new reference value of $h_{ref} = 1.29 \times 10^{-4}$ Btu/ft^{2}s-R . When applied to Eq (15), however, the reference calculation is unchanged because the fluid properties are determined at the reference temperature, $T^* = 670$ R . As a result, the low temperature viscosity problem is only consi-

derable when using the basic flat plate theory.

The boundary layer solution by numerical technique is accomplished by the boundary layer program referenced in Appendix B. Reading the freestream conditions of Mach Number M_∞, temperature T_∞, Prandtl Number Pr (as assumed earlier), and specific heat ratio γ (assumed as $\gamma = 1.4$ in all cases), the program yields the local Stanton Number St_x from which the local heat transfer coefficient is derived. The reference value given by this method is $h_{ref} = 9.5 \times 10^{-5}$ Btu/ft^{2}s-R for a wall temperature of $T_w = 580$ R , and $h_{ref} = 9.55 \times 10^{-5}$ Btu/ft^{2}s-R for a wall temperature of $T_w = 560$ R . A review of the program calculation revealed that the recovery factor was not accounted for in estimating the temperature potential. In hypersonic calculations, this recovery factor r is generally assumed as $r = 0.9$. According to Holman (Ref 8:213) as well as others, for laminar flow, $r = \sqrt{Pr}$. Assuming $Pr = 0.72$, then $r = 0.85$. Recalculation of the program value of reference heat transfer coefficient by each of these yields $h_{ref} = 1.21 \times 10^{-4}$ Btu/ft^{2}s-R for $r = 0.85$, and $h_{ref} = 1.11 \times 10^{-4}$ Btu/ft^{2}s-R for $r = 0.9$. The latter of these is consistent with the theoretical values. All remaining estimations will be based on a reference of $h_{ref} = 1.1 \times 10^{-4}$ Btu/ft^{2}s-R as it is consistent with theory and with the original test reference. Additionally, a recovery factor of $r = 0.9$ will be used in all subsequent calculations, both numerical and analytical. This is consistent with the original data reduction also.

An important consideration of the varying surface temperature, or nonisothermal wall effect, is the streamwise variation of heat transfer coefficient beyond the temperature step. The distance downstream over which this effect is felt must be well defined in order to accurately evaluate heat transfer beyond the wall temperature discontinuity. The variation of the heat transfer coefficient for an isothermal wall is then needed for comparison. According to Eckert high speed theory, Eq (15), this variation is shown in Fig 14. As indicated, the heat transfer coefficient decreases hyperbolically from the leading edge and levels out downstream. A comparison is given in Fig 15 between heat transfer coefficient calculations according to Eckert high speed theory and the boundary layer program for both Sutherland and low temperature viscosity. As shown, the variation of heat transfer coefficient is consistent with that indicated in Fig 14. Note that these values correspond to the isothermal wall case at zero deflection.

Isothermal Wall Calculations

In the reference calculations above, the various flat plate theory relations collapsed to one expression, as did the high speed theory equations, since the boundary layer edge values match the freestream values with no deflection of the plate. At a given deflection, however, an oblique shock occurs at the leading edge of the plate and the boundary layer edge conditions are no longer the freestream properties. The properties at the boundary layer edge are derived from the oblique

shock relations based on freestream conditions. Using these values, the various relations derived for flat plate theory, Eqs (10), (13), and (14), are revealed to diverge drastically. Similarly, the results gained from the definitions of Eqs (15)-(17) for high speed flow bear some disagreement. Using the boundary layer edge conditions, the boundary layer program revealed isothermal wall results which proved to be very consistent with the Eckert high speed calculation of Eq (15). Due to this correlation between theory and the numerical solution, Eq (15) has been found to be the correct expression of the Eckert theory, with the definition of Stanton Number given in Eq (2). The corresponding low speed expression is that given by Eq (10). The results of Eqs (13) and (14) for low speed flow, and of Eqs (16) and (17) for high speed flow were found to be unacceptable when compared to the numerical solution. The correspondence between theory and numerical solution is given in Fig 16. Also of note are the exactness of the approximation given by Eq (18) and the divergence between the low speed and high speed theoretical solutions at increasing deflection angles. Again, the numerical solution verifies the high speed theory in application to this problem. The correspondence between theory and numerical analysis lends further support to the correction of the program for a recovery factor of $r = 0.9$.

The boundary layer program was modified as indicated in Appendix B to solve the exact equations using the low temperature viscosity calculation of Eq (30). Using the boundary

layer edge conditions, the program calculations revealed that the heat transfer coefficient for the isothermal wall and low temperature viscosity did not diverge significantly from the Sutherland's Law calculations but agreed very closely. Calculation with Eq (15), Eckert high speed theory, agreed precisely with the boundary layer program for this case also. Fig 17 reveals the close correlation between theory and numerical solution once again. Note the divergence between high speed and low speed theory for increasing angle of deflection. A comparison of program data between Figs 16 and 17 reveals the close correlation for the two different viscosity calculations. This further supports the high speed theory based on Eckert's reference temperature. The high speed theory and the boundary layer isothermal wall calculations will be the basis of comparison for the nonisothermal wall boundary layer calculations.

V. Numerical Results

Nonisothermal Wall

Using the boundary layer program modified for a wall temperature step, as indicated in Appendix B, the numerical solution of the boundary layer equations can be derived for a constant temperature wall with a step change. This condition is the same as that assumed from the wind tunnel test data. The initial temperature of the wall is that gained from the thin skin test data at each deflection angle. For a deflection angle of $\alpha = 3$ degrees , a thin skin wall temperature of $T_w = 600$ R was extracted. Similarly, for $\alpha = 10$ degrees , $T_w = 620$ R , and for $\alpha = 14$ degrees , $T_w = 640$ R . These readings are also the basis of the isothermal wall calculations in the boundary layer program, as revealed in the previous section. As given earlier, the wall temperature over the HRSI material (assumed constant) is the new wall temperature after the step increase. For the deflection $\alpha = 3$ degrees , the wall temperature after the step is $T_{w2} = 700$ R . Similarly, for $\alpha = 10$ degrees , $T_{w2} = 760$ R and for $\alpha = 14$ degrees , $T_{w2} = 810$ R . Again, the ratio of heat transfer coefficient to the reference value is calculated for a streamwise location of $x/L = 0.575$.

Based on the given initial and final wall temperatures, the derived values of the ratio h/h_{ref} for the step change in wall temperature are given in Fig 18. The isothermal case, based on thin skin wall temperature at each angle of deflec-

tion, is given for comparison. Note that the nonisothermal wall result shows an increasing divergence from the isothermal case with increasing deflection angle. At a deflection of $\alpha = 3$ degrees , the nonisothermal case diverges from the isothermal by twelve percent while the divergence is nearly twenty percent at an angle of $\alpha = 14$ degrees . Also given for comparison are the HEATEST data results based on HRSI temperature data, and an equilibrium calculation based on HRSI temperature at a deflection angle of $\alpha = 3$ degrees . In this figure it is seen that the nonisothermal effects account for only about one-fourth of the discrepancy between the HEATEST data and the isothermal wall case at a deflection angle of $\alpha = 3$ degrees . However, at $\alpha = 14$ degrees , the HEATEST result is identical to the nonisothermal case.

For each angle of deflection studied, the variation of heat transfer coefficient with streamwise location is derived. As seen in Figs 19, 20, and 21, for $\alpha = 3$, 10, and 14 degrees , respectively, the isothermal data shows the same trends as indicated by the reference case in Fig 15. For each deflection angle, the streamwise location of the wall temperature step is $x/L = 0.467L$ where L is the plate length and is given to be $L = 1.25$ ft . According to the boundary layer program, the step increase in temperature creates a discontinuity in the heat transfer coefficient, after which it rises sharply, levels out quickly, and gradually decreases toward the trailing edge of the plate , as shown. After the discontinuity then, the heat transfer coefficient approaches

the condition of the isothermal case, but sees a discrete decrease in magnitude. The same is seen for all three deflection angles discussed. Note that the drop in heat transfer coefficient is sharper with increasing angle of deflection, and recovery toward the isothermal case is slower. Lastly, the magnitude of the difference between isothermal and nonisothermal cases is increasing with greater deflection angle, from about six percent of the isothermal value at the trailing edge at $\alpha = 3$ degrees to nine percent at $\alpha = 14$ degrees .

As indicated earlier, the change in results due to the low temperature viscosity relationship is very small since the case considered is at very high speed and thus has a high reference temperature. This is verified once again in calculating the nonisothermal wall case. Considering the values shown in Fig 22, there is very little difference between the isothermal values here and those shown in Fig 21. The same is true for the nonisothermal wall values for the ratio of of heat transfer coefficients. The same trends are shown as angle of deflection increases, with the divergence growing between isothermal and nonisothermal cases. Consequently, it has been shown through graphical results of the isothermal and nonisothermal wall calculations, and through the variation of heat transfer coefficient with location, that the low temperature viscosity calculation has shown no difference in the trends of behavior with location, deflection angle, or step presence, and very little difference in the magnitude of heat transfer coefficient ratio in any of these cases.

Step Size Variation

In reducing the test data, several considerations indicate that the step size and wall temperatures assumed may not be accurate. The effect of a lower wedge temperature, coupled with a higher HRSI surface equilibrium temperature, would cause a significant increase in step size, with associated boundary layer effects. A larger step size should certainly have an effect on the magnitude and recovery distance of the heat transfer coefficient. Thus, understanding the effects of a larger step would be beneficial in assessing the validity of conclusions drawn from other results. In addition, increasing the step size makes the test results more versatile, and more broadly applicable to a range of considerations.

To investigate the effect of increasing the step size, the step used previously in each deflection angle case was incremented. The heat transfer coefficient variation was derived for a step of twice the original step, four times the original step, and twice the initial wall temperature. This was accomplished for each deflection angle. The results for a deflection angle of α = 3 degrees are plotted in Fig 23, for α = 10 degrees in Fig 24, and for α = 14 degrees in Fig 25. For the case of deflection angle α = 3 degrees , the heat transfer coefficient sees a sharp discontinuity for all cases. This discontinuity grows with step size. For smaller steps, the heat transfer coefficient rises sharply, peaks, and decreases gradually toward the trailing edge. For increasing step size, the minimum value is no longer seen

immediately, but comes more gradually as heat transfer coefficient falls more slowly, then recovers more slowly. For the step size of four times the original step size, a peak is not reached until $x/L = 0.8$. For still larger steps, the peak may not be reached. Generally, reaction of heat transfer coefficient is slower for increasing step size, while minimum value is smaller and magnitude downstream is smaller. This is also seen to be true for the same increments of step size at deflections of $\alpha = 10$ and 14 degrees . In addition, note that reaction and recovery are slowing, and magnitude decreasing as the deflection angle increases, as noted earlier and emphasized with this data.

The size of the step can also be changed by lowering the initial wall temperature. This is consistent with the lower temperature expected on the stainless steel wedge, as mentioned previously. Indeed, from experience, the wedge temperature may remain very close to its initial temperature. For the deflection angle $\alpha = 3$ degrees , the surface temperature initially is $T_{w1} = 540$ R , and at $\alpha = 14$ degrees , the surface temperature is $T_{w1} = 550$ R . Using these initial wall temperatures, with the HRSI final temperature for the appropriate deflection angle, yields the streamwise distribution of heat transfer coefficient for $\alpha = 3$ and 14 degrees in Figs 26 and 27, respectively. The heat transfer coefficient ratio for each deflection angle is shown in Fig 18. These values reveal that at a deflection angle of $\alpha = 3$ degrees , the nonisothermal wall accounts for about

forty percent of the discrepancy, while at a deflection of α = 14 degrees , about sixty percent is accounted for, as seen in Fig 18. These results require some qualification. The initial wall temperature used here is the lowest value possible, before the wedge is subjected to any heat transfer. This should be reasonable for the low angle case, but is questionable in the higher angle case, where heating is significantly higher. Therefore, the reliability of the lower angle case is probably better. Comparing these values of the heat transfer coefficient ratio with Fig 28, the wall temperature step may have to be double that assumed here to account for the entire discrepancy. While the HRSI surface temperature may be higher than that indicated by the test data, it should be doubtful that it will be twice that indicated.

The variation of the ratio of heat transfer coefficients with increasing step size and angle of deflection is revealed in Fig 28. The isothermal wall case is given for comparison and all values are shown for a location of $x/L = 0.575$. As shown, there is no real pattern with increasing step size except that the magnitude is decreasing. Note, however, that the effect of recovery location is important. At deflection of α = 3 degrees , all but the largest step are fairly well recovered by $x/L = 0.575$. Only the magnitude of the largest step is very small. At an angle of α = 10 degrees , the step of four times the original step is at its minimum value at this x location, while the largest step is still approach-

ing minimum. The other smaller steps are well recovered. Finally, at $\alpha = 14$ degrees, neither of the two larger steps has reached a minimum, while the two smaller steps are recovering at $x/L = 0.575$. This serves to emphasize the delay in recovery for increasing step size and increasing deflection angle, as well as the decrease in heat transfer coefficient for increasing step size.

Step Location Variation

As an additional consideration, the effect of varying the step location has been investigated. The results are shown in Fig 29. This set of calculations was conducted using a constant temperature step with a constant initial wall temperature and fixed deflection angle. The conditions chosen were at a deflection angle of $\alpha = 3$ degrees , with the initial wall temperature of $T_{w1} = 600$ R , and a final wall temperature of $T_{w2} = 700$ R . Step locations were taken as $x/L = 0.1, 0.25, 0.47, 0.6$, and 0.8 . For the thermocouple location $x/L = 0.575$, only those step locations upstream would affect the heat transfer coefficient seen. However, from the results it is seen that recovery is somewhat slower as the step is moved downstream. Additionally, the drop in heat transfer coefficient is larger with increasing x location. Finally, the magnitude of the deviation from the isothermal case seems to increase downstream, although it doesn't become very large with the given step size. The overall effect is to increase recovery distance and deviation with increasing downstream step location.

VI. Results of Superposition Analysis

In an effort to verify the boundary layer program results analytically and at the same time identify the trends in variation of heat transfer coefficient with arbitrary wall temperature variations, a secondary means of estimating the nonisothermal effect was desired. An analytical method of estimating the heat transfer coefficient with the nonisothermal wall which was presented in the section on Theory is the superposition technique. This method was applied to the cases of deflection angle α = 3, 10, and 14 degrees , with the corresponding initial and final wall temperatures. As used in hypersonic theory calculations, the fluid properties were derived from the reference temperature for each case, and the recovery temperature was used in the temperature potential in place of the freestream temperature.

The results of this estimation method are given in Figs 30, 31, and 32, for the deflection angles of α = 3, 10, and 14 degrees , respectively. The data suggests several conclusions. The change in heat transfer coefficient from the isothermal distribution increases with deflection angle. Also, the superposition estimation does demonstrate great discontinuity effects. A sharp drop and recovery are shown in each case, increasing in magnitude with deflection angle. This effect is similar to that demonstrated by the numerical solution.

The results yielded by the numerical and analytical

methods are compared in Fig 33. The methods of numerical solution and superposition are compared to the isothermal wall case calculated by the boundary layer program and Eckert high speed theory. The values shown represent the ratio of heat transfer coefficient at the streamwise location $x/L = 0.575$, for varying deflection angle. As seen, the numerical solution yielded the greatest divergence from the isothermal wall calculations. This divergence ranges from a value of 12 to 19 percent of the isothermal value. By comparison, the range of divergence shown for the superposition method is between 6 and 13 percent. The result is that the analytical results given by wall temperature superposition reveal consistent trends in the heat transfer coefficient change due to the wall temperature discontinuity, at varied deflection angles. However, the magnitude of this effect is consistently smaller according to superposition than that indicated by numerical solution. The values derived from each method do form a small range of values in which the nonisothermal wall effect may be expected to fall, with the limits of this range formed by the superposition estimation at the upper limit and the numerical solution at the lower limit.

VII. Conclusions and Recommendations

Conclusions

Experimental Data. The test data revealed several uncertainties that left the actual step size unknown. At a deflection angle of $\alpha = 3$ degrees , the HRSI test article reached equilibrium. At $\alpha = 10$ and 14 degrees , this condition was not achieved. The HRSI temperature used for these cases was lower than that required for equilibrium. The thermocouple itself was not at the surface but beneath the radiative coating. The associated temperature reading may have been lower than the actual surface temperature. The constant surface temperature assumption for the HRSI article appears valid. The stainless steel wedge surface temperature was not necessarily equal to the appropriate thin skin plate surface temperature. This is strongly indicated by the heat sink argument and by the thin skin heat transfer coefficient data cited. Constant temperature on the wedge was assumed but could not be verified. The conclusions from this data is that initial wall temperature should be lower than the thin skin data used. HRSI equilibrium surface temperature should be higher, especially for the higher deflection angle cases. The overall step was significantly larger than that assumed from thin skin and HRSI test data.

Reference Conditions. In calculating the reference value of the heat transfer coefficient, Eckert high speed flat plate theory proved to be consistent with the boundary layer pro-

gram. Evaluation of program results considering recovery temperature showed precise correlation between numerical and analytical reference solutions, assuming a recovery factor of $r = 0.9$. This was consistent with the original data reduction as well. Low speed theory diverged drastically at high deflection angles and was proven inappropriate. In high speed theory based on Eckert's reference temperature, low temperature viscosity shows no divergence. High speed theory is valid according to test conditions and correlation with numerical results. The numerical solution and Eckert theory yield the isothermal wall solution used for comparison.

Numerical Results. Numerical calculation for the nonisothermal wall showed a divergence from the isothermal case accounting for 28 percent of the discrepancy cited at a deflection angle of $\alpha = 3$ degrees . Originally, this calculation also accounted for 100 percent of the discrepancy at $\alpha = 14$ degrees . However, according to the study accomplished by Woo (Ref 9), the experimental data consistently yielded a ratio of heat transfer coefficient to reference of $h/h_{ref} = 2.4$. With this discrepancy value, the nonisothermal wall accounted for 41 percent of the deviation. The step size in the above cases was derived directly from the thin skin and HRSI test data. The step size was varied to model possible wall temperature conditions. The final wall temperature was varied by doubling and quadrupling the initial step size and by doubling the initial wall temperature for all deflection angles considered. The result of increasing magnitude

of the step is a significant decrease in heat transfer coefficient, and increase in the downstream distance affected by the wall temperature discontinuity.

The initial wall temperature was varied to model the lower surface temperature expected on the stainless steel wedge. The initial wall temperature assumed the value of the initial thin skin temperature, with the final wall temperature taken from the appropriate HRSI data. These runs were expected to best correlate the actual wall temperature discontinuity in the wind tunnel tests. The result showed the nonisothermal wall effect accounted for 40 percent of the discrepancy at α = 3 degrees , and 60 percent at α = 14 degrees . Accordingly, the wall temperature step would have to be twice its expected value to account for the entire discrepancy.

The location of the step was varied to investigate the effect of flow development on the heat transfer coefficient. The divergence of the heat transfer coefficient from the isothermal case grew with increasing distance downstream. Response also seemed slower for the aft step locations.

The results of the numerical calculations are valid as long as the boundary layer assumptions are valid. However, in the area of the wall temperature discontinuity, the boundary layer solution is not valid due to axial diffusion and three dimensional effects. In the area of the discontinuity, the numerical results are questioned. Away from this discontinuity, the boundary layer solution should be reliable. The effect of diffusion near the discontinuity may be a delay in

recovery of the heat transfer coefficient to a point further downstream. In addition, three dimensional effects at the surface around the discontinuity may keep the tile surface temperature closer to the original wall temperature. The effective step may be delayed such that the location of the thermocouple may be in the region of steep heat transfer coefficient recovery. The combined effects of these characteristics would be a significantly lower heat transfer coefficient reading at the thermocouple location, possibly still accounting for the entire discrepancy.

Analytical Results. Analytical solution of the boundary layer with the nonisothermal wall condition was accomplished by wall temperature superposition. The superposition method revealed similar effects of the nonisothermal wall to those shown by the numerical solution. However, some magnitude discrepancy was shown between the numerical and analytical methods. Again, the analytical methods assume boundary layer conditions and may not be valid near the wall temperature discontinuity.

Discussion of Results. The results of this study with respect to the original problem posed are summarized. The nonisothermal wall effect does account for much of the experimental data discrepancy, with as much as half of the discrepancy accounted for. Since exact surface temperature distribution is unknown on the HRSI tile, the wall temperature step is still not completely defined. The lowest possible temperature on the stainless steel wedge is the thin skin

initial temperature. The wedge surface is expected to have been very close to this temperature throughout the run. The step size was probably very close to that used in the initial wall temperature variation calculations. This result showed the nonisothermal wall accounting for roughly half of the original discrepancy. The HRSI temperature may have been somewhat higher on the surface than the data indicated. The possible delay in heat transfer coefficient response due to axial diffusion and due to three dimensional effects at the surface may be an additional effect not accounted for. Since the thermocouple location is near the wall temperature step location, the temperature reading may have been in the region of the heat transfer coefficient recovery. A much lower value of this coefficient could result. However, the final conclusion of these findings is that only one-half of the discrepancy may actually be attributed to the nonisothermal effect, pending further investigation. The remaining portion may be due to the diffusion effect, three dimensional effects, inaccuracy in thermocouple data, fluctuations in boundary layer and surface heating ahead of the tile, and/or inaccuracy in data reduction. While the radiation heat transfer was also cited as a possible cause earlier, the HRSI temperature should not vary greatly from the thermocouple data. As a result, radiation analysis should serve to verify the test data, at best.

Applications. The results of this study may be applied beyond the scope of the original problem. The effect of the

nonisothermal wall is present in a number of applications, particularly in high speed flow. On any high speed vehicle, discontinuity in surface material results in temperature discontinuity. This is especially true of the Space Shuttle Orbiter. Several locations are marked by a change in surface material on this vehicle. At the nosecap, the surface is insulated with Reusable Carbon-Carbon (RCC) material, followed by HRSI surface insulation. The Carbon-Carbon acts as a heat sink while the HRSI is an insulator. As such, the initial temperature should be lower than the HRSI surface temperature, and a wall temperature step is present. The data presented here qualitively describes the fluctuation of heating due to this discontinuity, depending on the relative magnitude of the RCC and HRSI surface temperatures. Similar surface material changes occur at other locations. The lower surface points of attachment to the External Tank (ET) are marked by an HRSI, RCC, stainless steel, RCC, HRSI sequence of materials. The heating characteristics near these points should reflect a compounded nonisothermal wall effect. On the OMS pod, a Low-temperature Reusable Surface Insulator (LRSI) to FRSI material change occurs. Again, a wall temperature step occurs, with the associated effects. Of course, the flow is further complicated by changing boundary layer edge conditions over the vehicle, but the demonstrated nonisothermal wall effect will greatly influence the surface heating at many locations on the vehicle.

Recommendations

As discussed above, numerous questions remain unanswered. The temperature distribution is unknown on the surface of the stainless steel wedge. In order to completely define the wall temperature and investigate the full effects, the surface temperature ahead of the test article location should be investigated. This may be accomplished through experimental tests at all deflections using thermocouple measurements, or through a thorough analytical model of the material conductive and radiative properties based on flow conditions. The result of this investigation would be better knowledge of the temperature distribution and subsequent effects of the wall temperature variation on heating. The HRSI surface temperature should also be verified, since the test thermocouple data was taken beneath the radiative coating. In addition, knowledge of the surface temperature of the HRSI tile near the surface material change would indicate the location of the effective step and help to further model the heat transfer coefficient variation. Again, thermocouple test data could be used.

The wall temperature of the wind tunnel during the experimental runs would have served to validate the HRSI surface temperature distribution. Without knowledge of the tunnel wall temperature, equilibrium heating could not be fully determined. This prevented knowledge of HRSI surface temperature, especially at the higher deflection angles. This should be investigated by experimental observation.

The boundary layer assumptions were considered invalid at the discontinuity. As a result, the results near the discontinuity may not be reliable. A complete Navier-Stokes solution of the boundary layer should be accomplished to determine the limits of validity of the boundary layer solution, to verify the numerical results at all locations, and to investigate further the complete nonisothermal wall effect.

Possible errors cited include thermocouple inaccuracy, data reduction inaccuracy, and conduction in the tile. The reliability of thermocouple data in high speed testing is inherent to the accuracy and validity of test results in all applications. Errors caused by mounting, location, and conduction should be investigated. Conduction in the tile material is perhaps the most important property of the insulator since it determines the capability to protect the Orbiter during reentry. All conductive effects must be understood, particularly those due to irregularities in the coating, in mounting, and in construction of the tile itself. Further investigation is needed in this area. The study of Woo (Ref 9) has served to verify the accuracy of the data reduction technique. Validation of the technique for known results may further verify its reliability.

Lastly, many applications of the nonisothermal wall exist. A parametric study of wall temperature variation effects on heating should be conducted with the emphasis on applications. This would encompass a broad range of flow conditions, step locations, step sizes, and temperature distributions. The

result of this type of study would be enhancement of applicability of results to varied conditions and to a broader range of fields. The nonisothermal wall effect on heating could thus be better understood, recognized, and predicted in future applications.

Table I

HRSI Tile Run Description

File	Angle at Injection	Description
1	14 degrees	. . .hold . . 9 deg . . . hold . . 14 deg
2	14 degrees	. . .hold . . 9 deg . . . hold . . 14 deg
3	14 degrees	. . .hold . . 9 deg. . .no hold. . 14 deg
4	14 degrees	. . .hold . . 3 deg. . . .hold . . 14 deg
5	14 degrees	. . .hold . . 3 deg. . .no hold. . 14 deg
6	10 degrees	. . 3 deg . . 14 deg . . 3 deg . . 14 deg
7	14 degrees	. . .hold . . 3 deg . . .hold . . 14 deg
8	14 degrees	. . .hold . . 9 deg. . .no hold. . 14 deg
9	Pitch error, file scratched.	
10	14 degrees	. . .hold . . 9 deg. . . .hold . . 14 deg
11	10 degrees	. . 3 deg . . hold . . . .hold . . 10 deg
12	14 degrees	. . .hold . . hold . . . .hold . . hold
13	14 degrees	. . .hold . . 3 deg. . . .hold . . 14 deg
14	10 degrees	. . 3 deg . .14 deg. . . 3 deg . . 14 deg
15	10 degrees	. . .hold . . shock generator . . hold
16	10 degrees	. . 3 deg . . hold . shock generator . .
17	14 degrees	. . .hold . . shock generator . . hold
18	14 degrees	. . .hold . . 3 deg. . . .hold . . 14 deg
19	14 degrees	. . .hold . . hold . . . .hold . . . . .
20	10 degrees	. . .hold . . hold . . . .hold . . . . .
21	10 degrees	. . 3 deg . . hold . . . .hold . . . . .
22	14 degrees	. . .hold . . 9 deg. . . .hold . . 14 deg
23	14 degrees	. . .hold . . 9 deg. . . .14 deg . . . .

Table II

FRSI Tile Run Description

File	Angle at Injection	Description
27	14 degrees	. . . hold . . . hold . . . hold . . . .
28	10 degrees	. . . hold . . . hold . . . hold . . . .
29	10 degrees	. . . 3 deg . . hold . . . hold . . . .
30	10 degrees	. . . hold . . . hold . . . hold . . . .
31	14 degrees	. . . hold . . . 9 deg . . hold . . 14 deg
32	14 degrees	. . . hold . . . 9 deg . . 14 deg . . .
33	14 degrees	. . . hold . . . 3 deg . . hold . . 14 deg
34	14 degrees	. . no hold . . 3 deg . . 14 deg . hold
35	14 degrees	. . no hold . . 3 deg . . hold . . 11.6 deg
36	10 degrees	. . . 3 deg . . hold . shock generator . .
37	10 degrees	. . . hold . . . shock generator . . . .
38	14 degrees	. . . hold . . . shock generator . . . .
39	14 degrees	. . . hold . . . 3 deg . . hold . . 14 deg
40	14 degrees	. . . hold . . . 3 deg . no hold . 14 deg
41	14 degrees	. . . hold . . . hold . . . hold . . . .
42	10 degrees	. . . hold . . . shock generator . . . .
43	10 degrees	. . . hold . . . shock generator . . . .
44	10 degrees	. . . hold . . . shock generator . . . .
45	14 degrees	. . . hold . . . shock generator . . . .

Table III

Thin Skin Run Description

File	Angle at Injection	Description
46	14 degrees	. . . hold . . . hold . . . hold . . .
47	14 degrees	. . . hold . . shock generator . . . .
48	14 degrees	. . . hold . . . hold . . . hold . . .
49	14 degrees	. . . hold . . shock generator . . . .
50	14 degrees	. . . hold . . shock generator . . . .
51	14 degrees	. . . hold . . shock generator . . . .
52	14 degrees	. . . hold . . shock generator . . . .
53	14 degrees	. . . hold . . shock generator . . . .
54	10 degrees	. . . hold . . shock generator . . . .
55	10 degrees	. . . hold . . shock generator . . . .
56	10 degrees	. . . hold . . shock generator . . . .
57	10 degrees	. . . hold . . . hold . . . hold . . .
58	10 degrees	. . . hold . . . 3 deg . . hold . . .
59	10 degrees	. . . 3 deg . . hold . shock generator

Table IV

Conditions for Computational and Analytical Cases

Fig	α (deg)	T_{w1}	T_{w2}	$2x\Delta T$	$4x\Delta T$	$2xT_{w1}$
19	3	600	700			
20	10	620	760			
21	14	640	810			
23	3	600	700	800	1000	1200
24	10	620	760	900	1180	1240
25	14	640	810	980	1320	1280
26	3	540	700			
27	14	550	810			
29	3	600	700			
30	3	600	700			
31	10	620	760			
32	14	640	810			

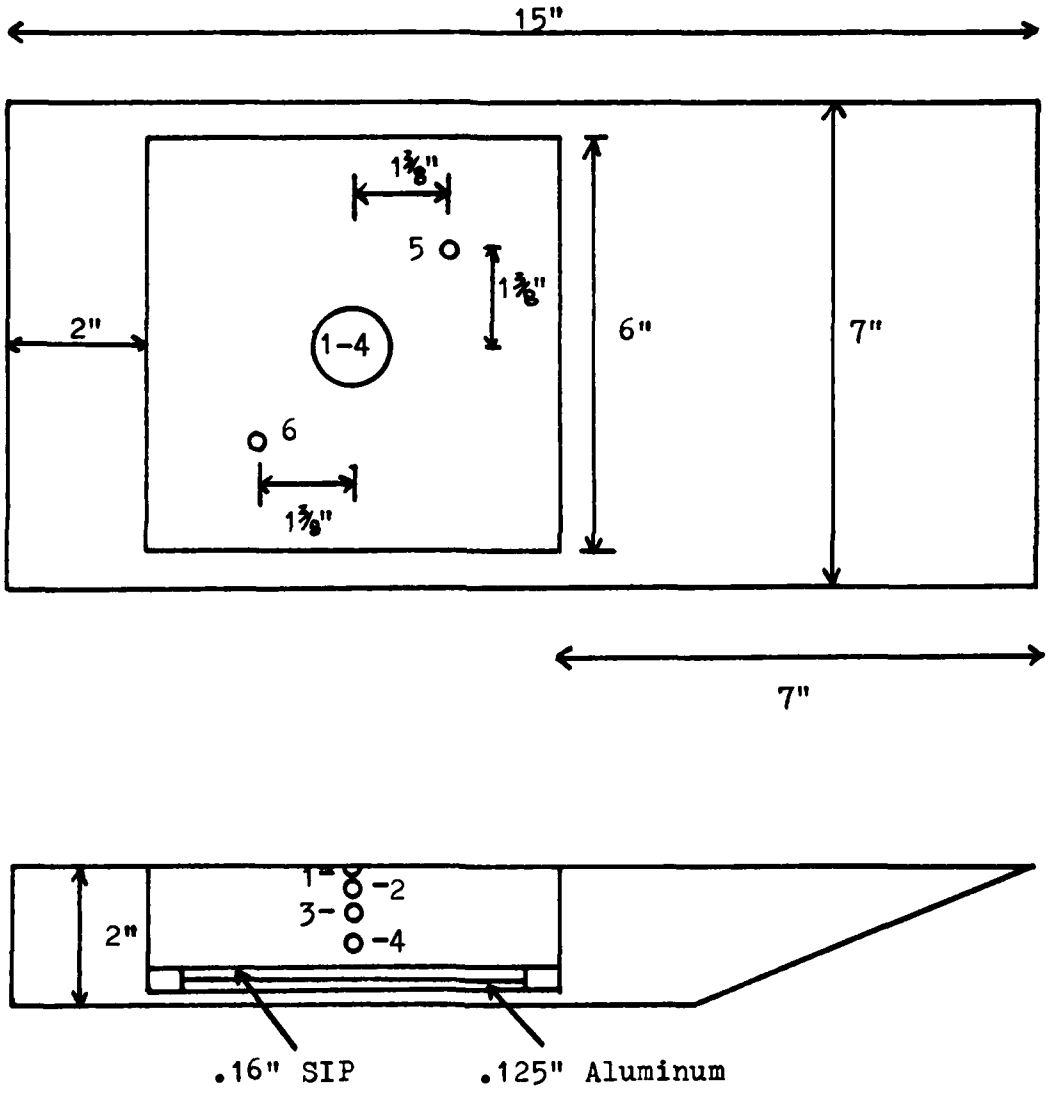

Figure 1. HRSI Test Apparatus

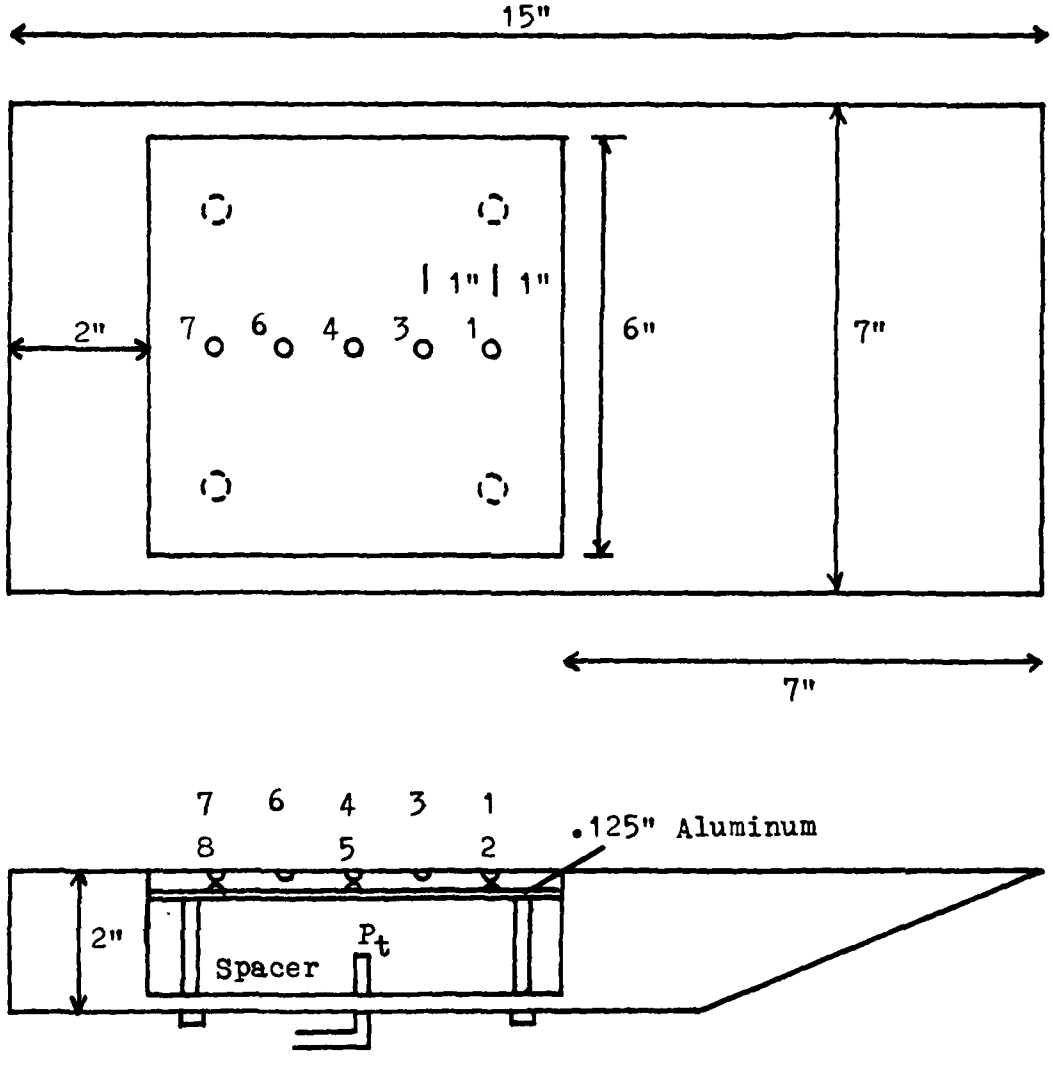

Figure 2. FRSI Test Apparatus

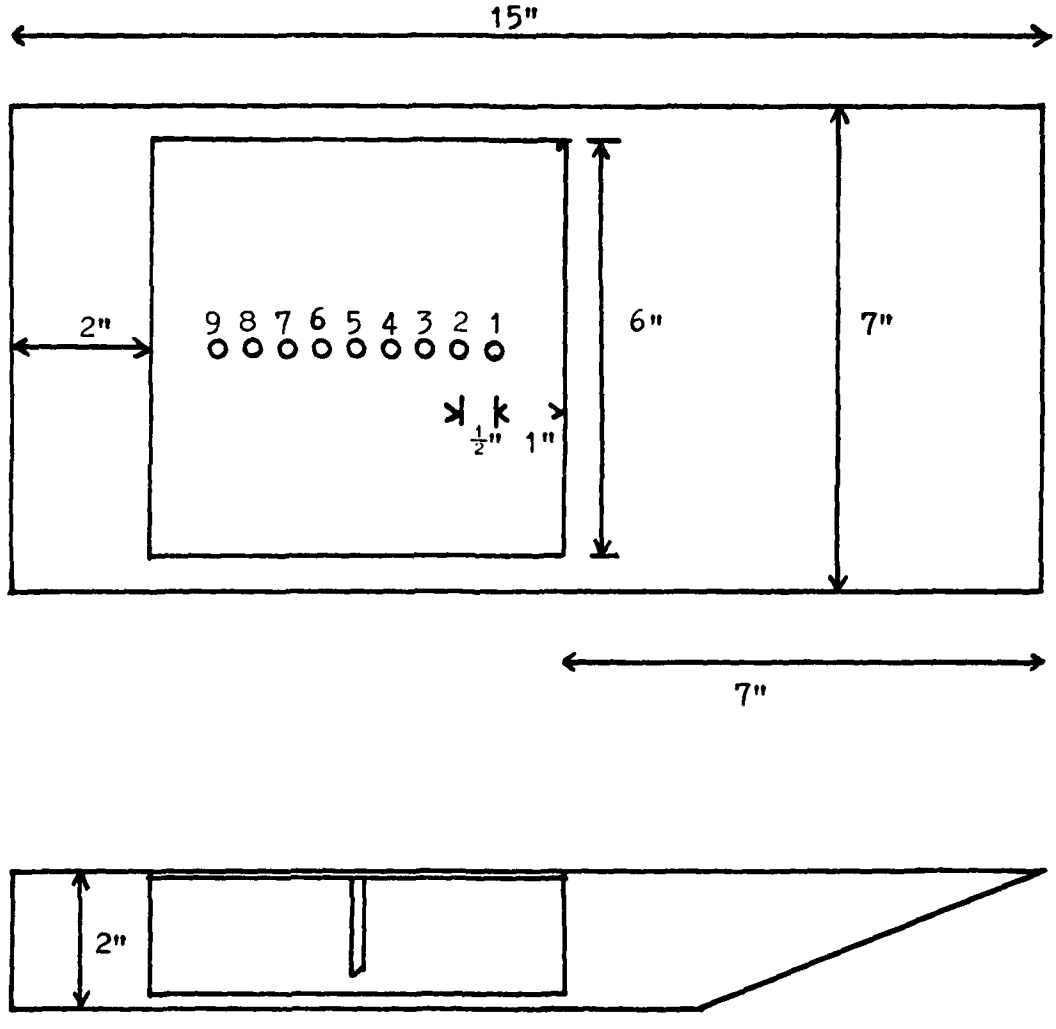

Figure 3. Thin Skin Test Apparatus

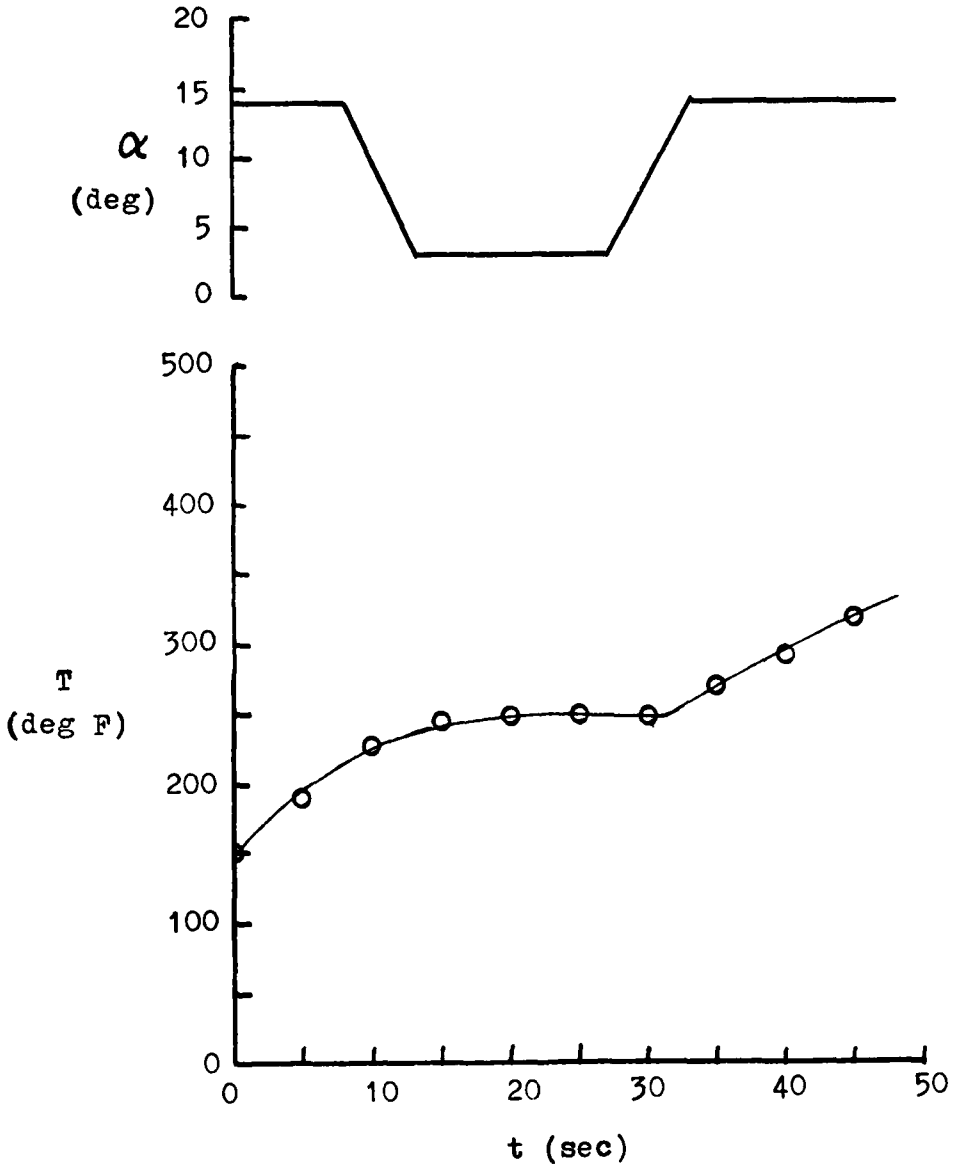

Figure 4. Wind Tunnel Thermocouple Data for Transient Maneuver (Mach 14.25) (Ref 1)

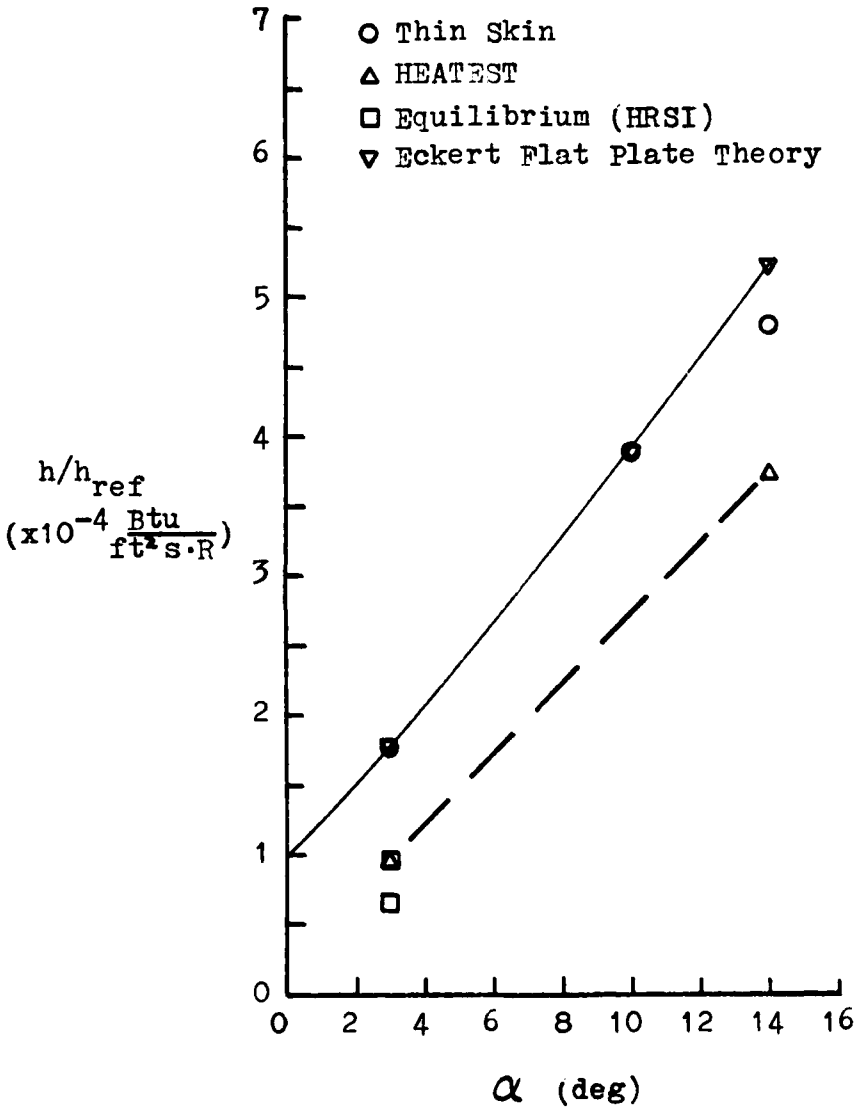

Figure 5. Heating Estimate for Wind Tunnel Thermocouple Data (Transient Maneuver) (Ref 1)

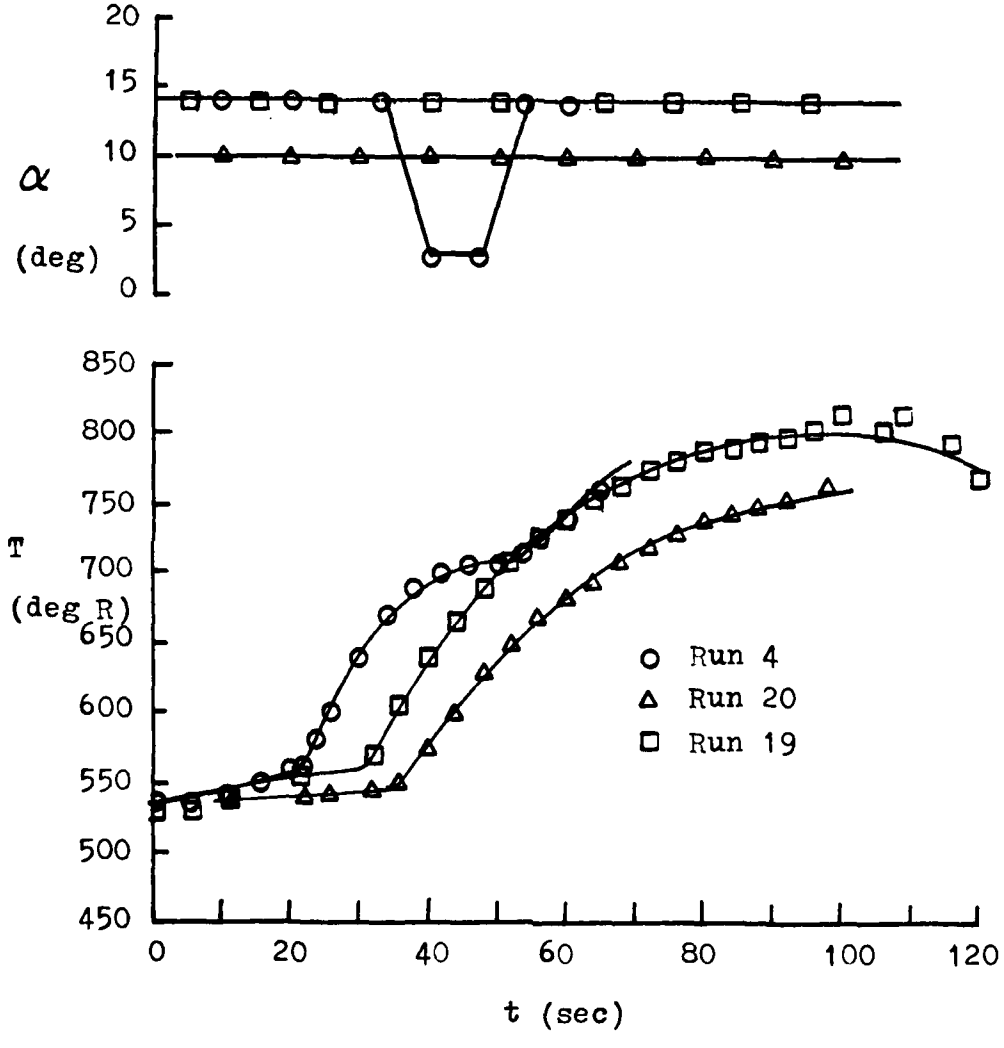

Figure 6. Thermocouple Data for HRSI Test Runs

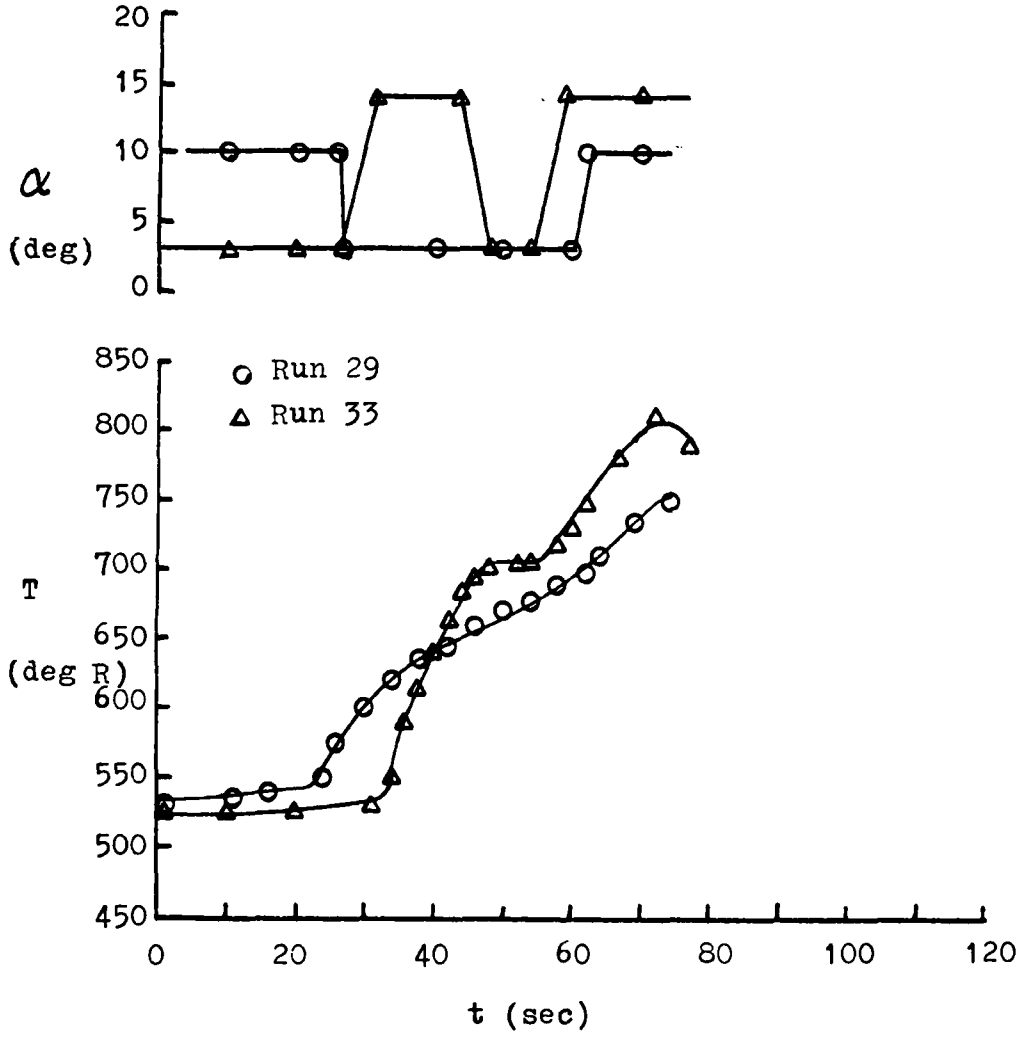

Figure 7. Thermocouple Data for FRSI Test Runs

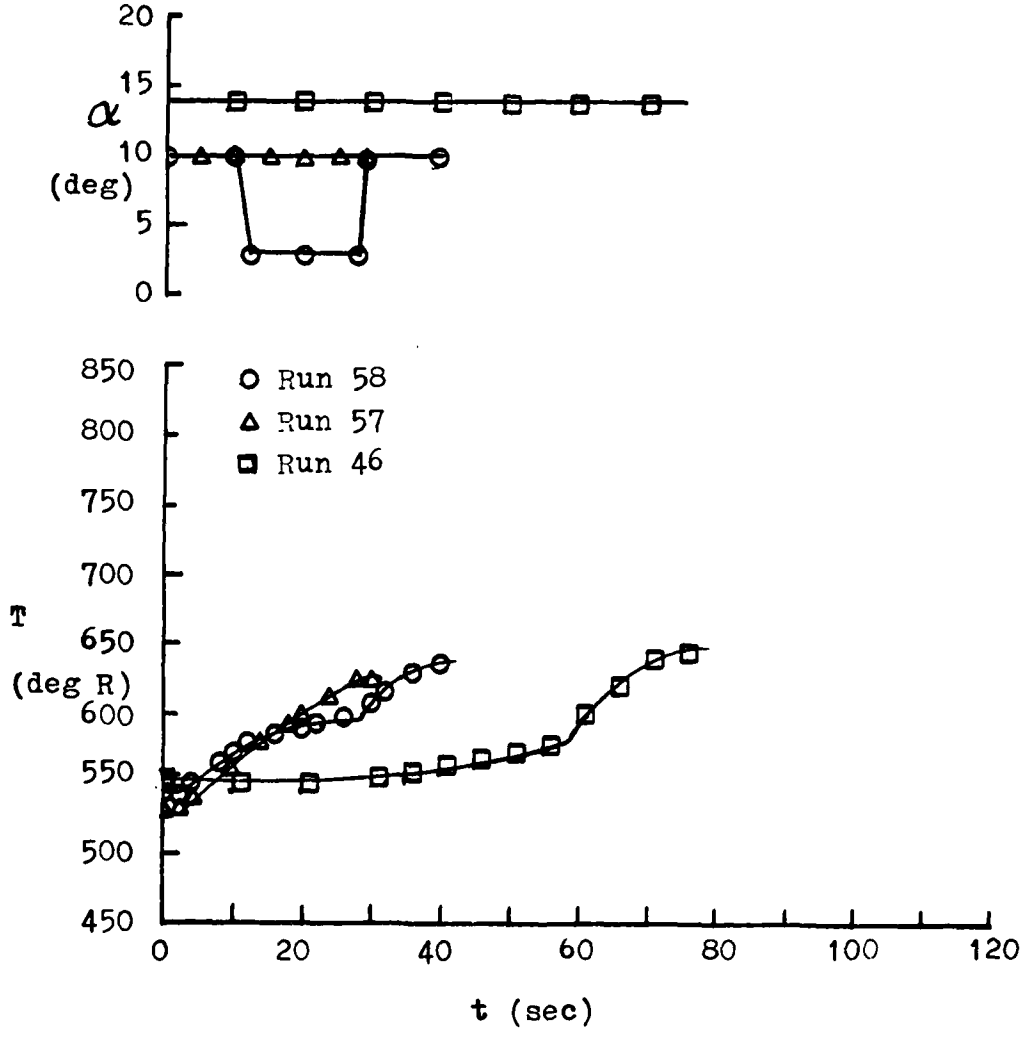

Figure 8. Thermocouple Data for Thin Skin Test Runs

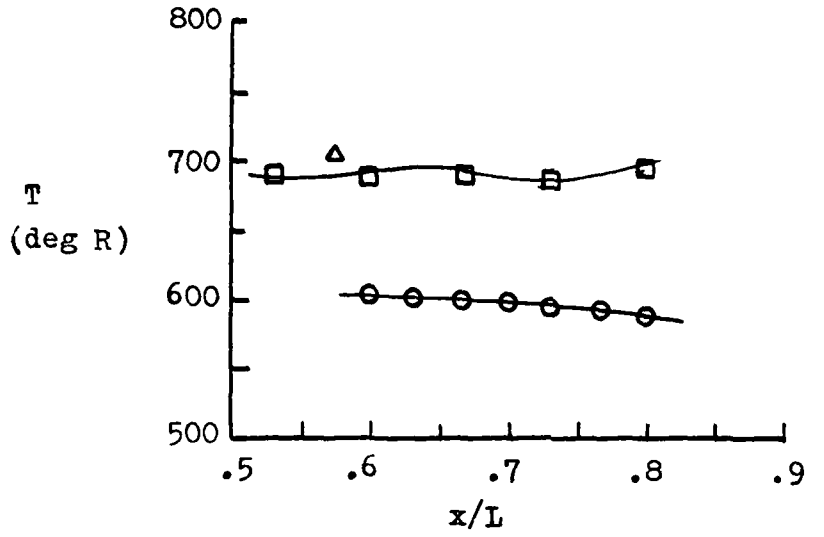

Figure 9. Wind Tunnel Thermocouple Data Distribution (α = 3 degrees)

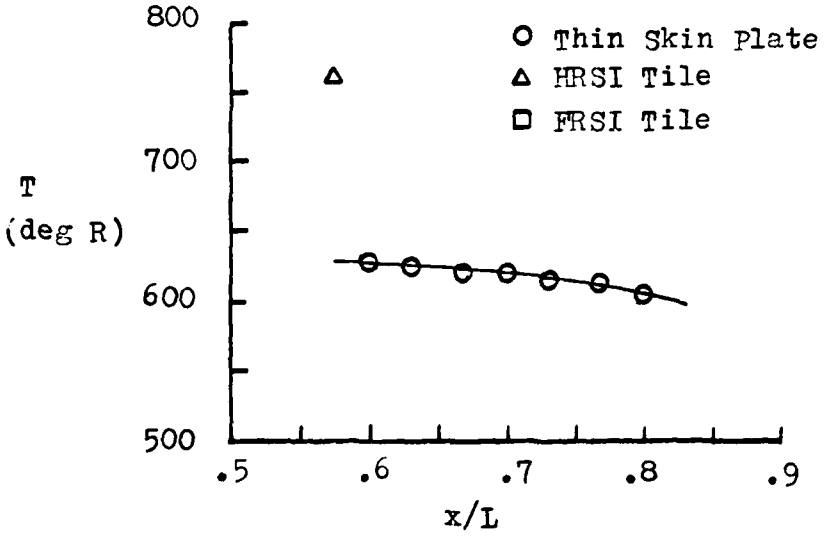

Figure 10. Wind Tunnel Thermocouple Data Distribution (α = 10 degrees)

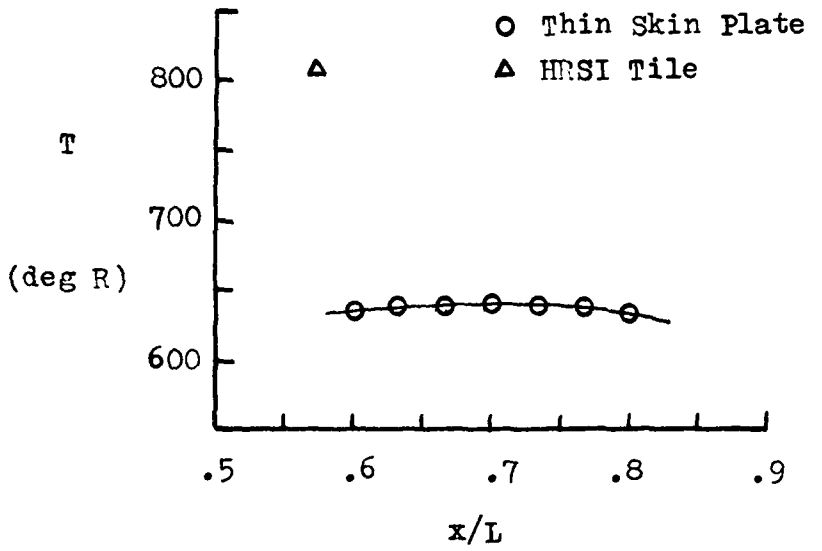

Figure 11. Wind Tunnel Thermocouple Data Distribution (α = 14 degrees)

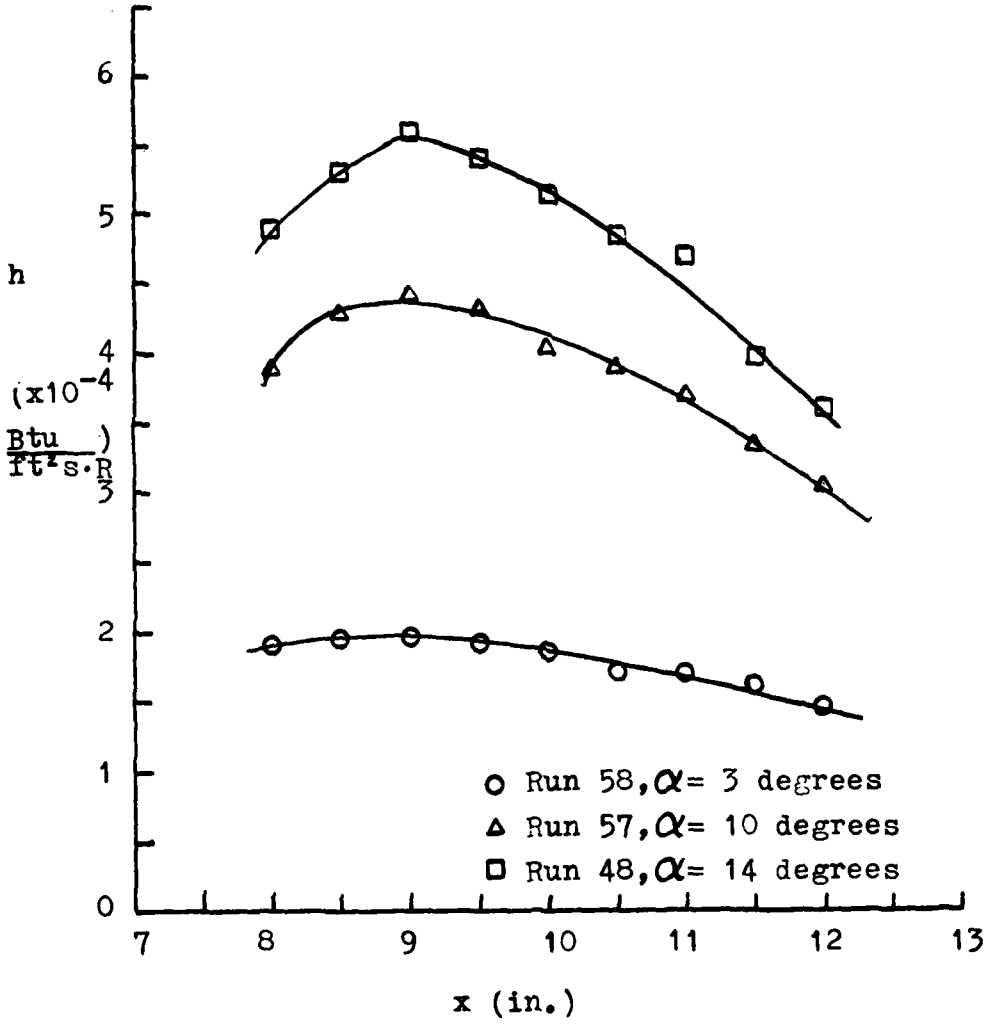

Figure 12. Experimental Heat Transfer Coefficient Distribution from Thin Skin Wind Tunnel Tests

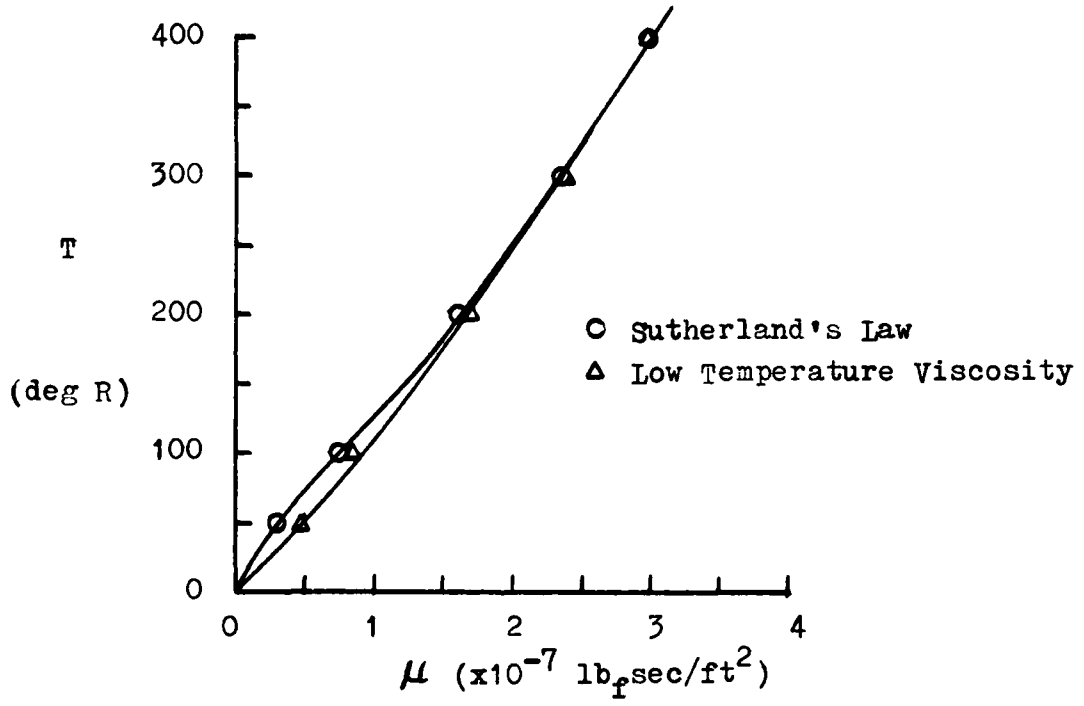

Figure 13. Comparison of Sutherland's Law and Low Temperature Calculations of Viscosity

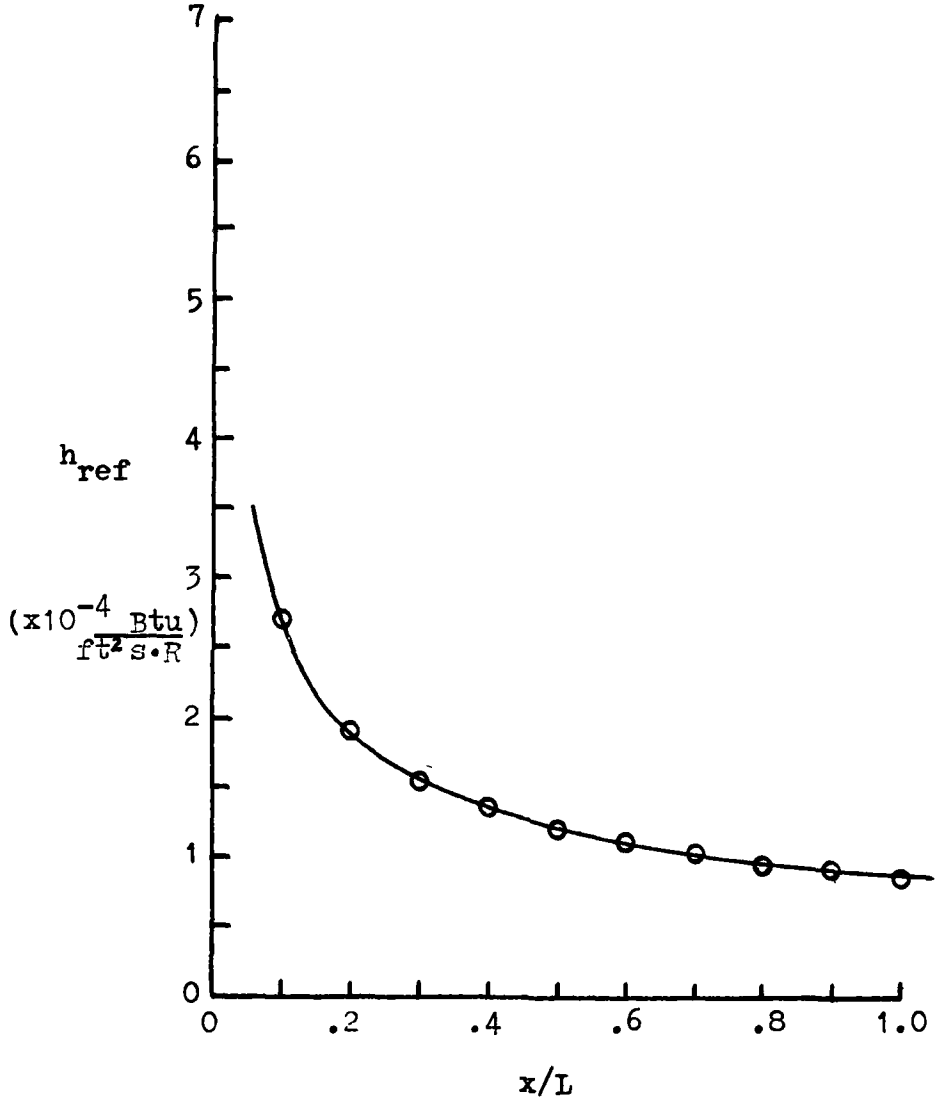

Figure 14. Streamwise Distribution of Reference Heat Transfer Coefficient

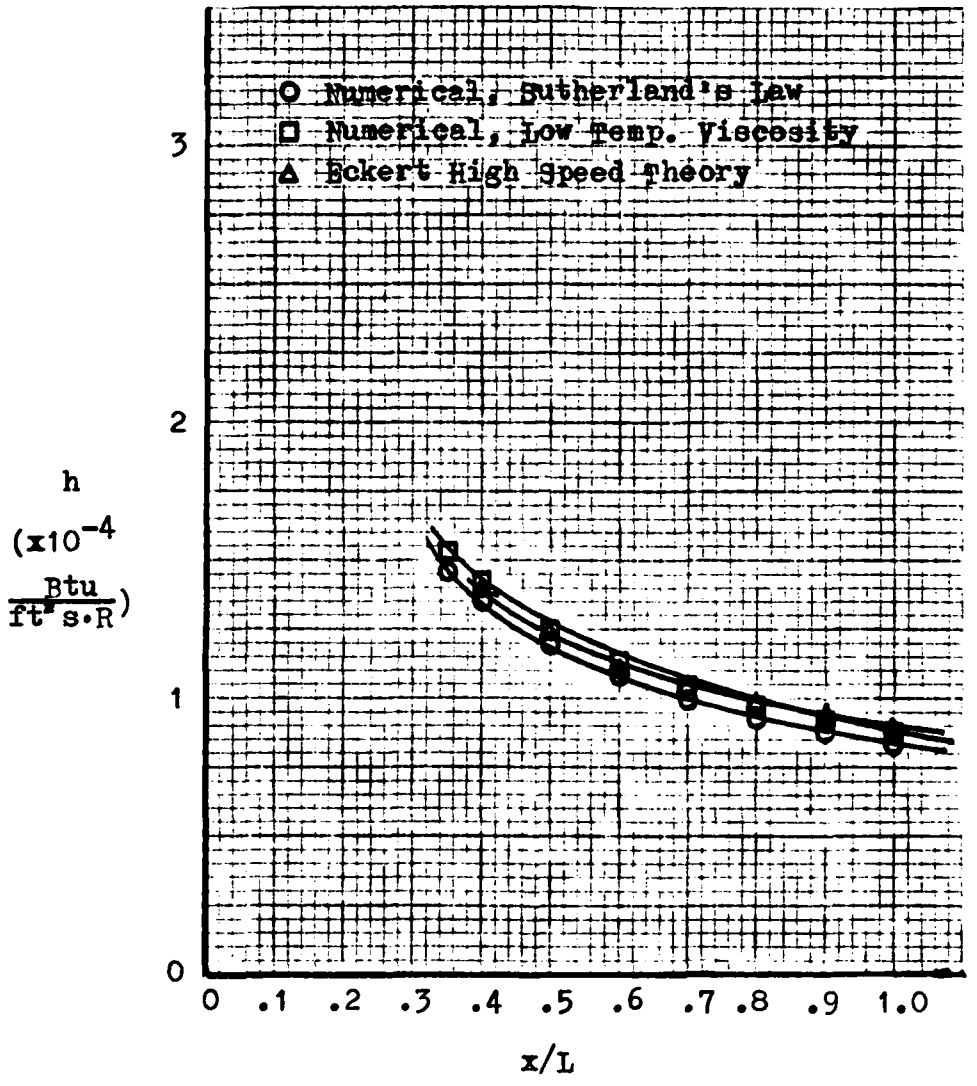

Figure 15. Comparison of Streamwise Distribution of Reference Heat Transfer Coefficient

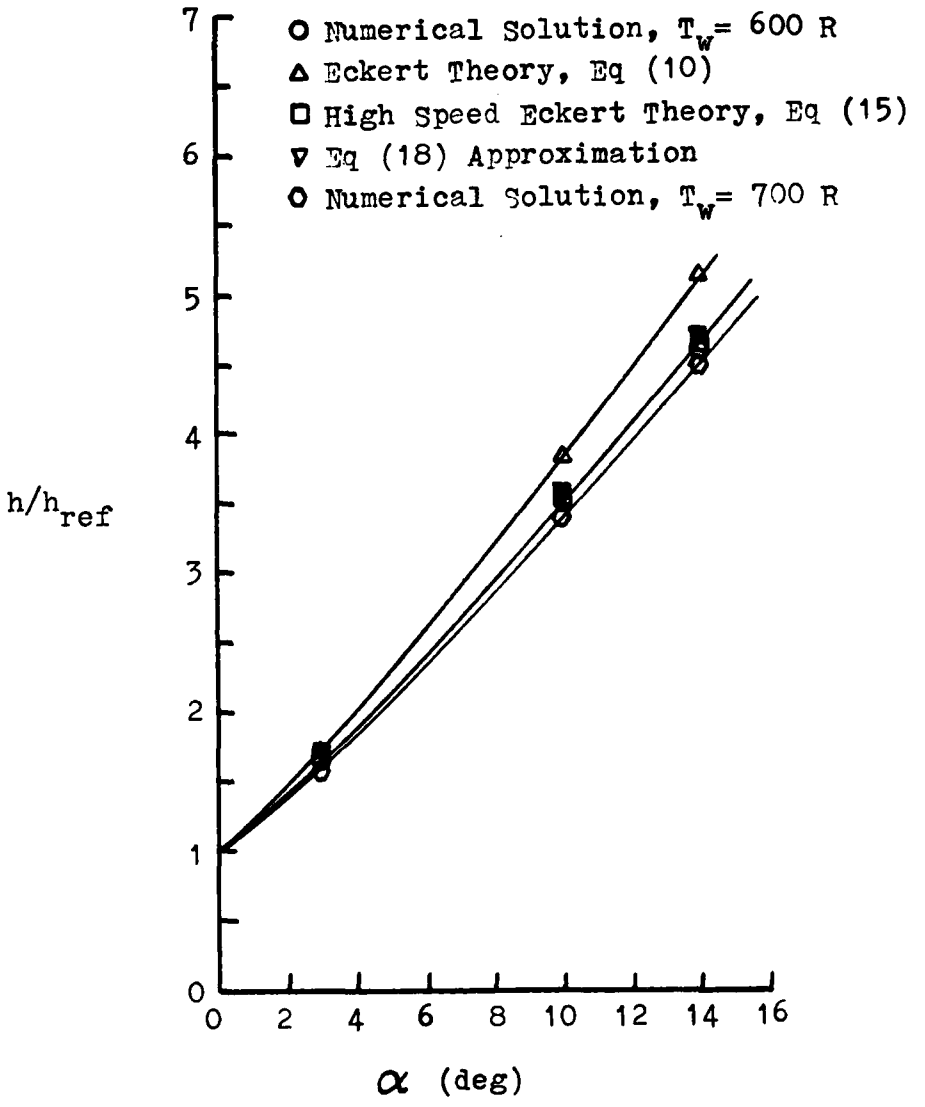

Figure 16. Comparison of Isothermal Wall Heat Transfer Coefficient Calculations (x/L = 0.575)

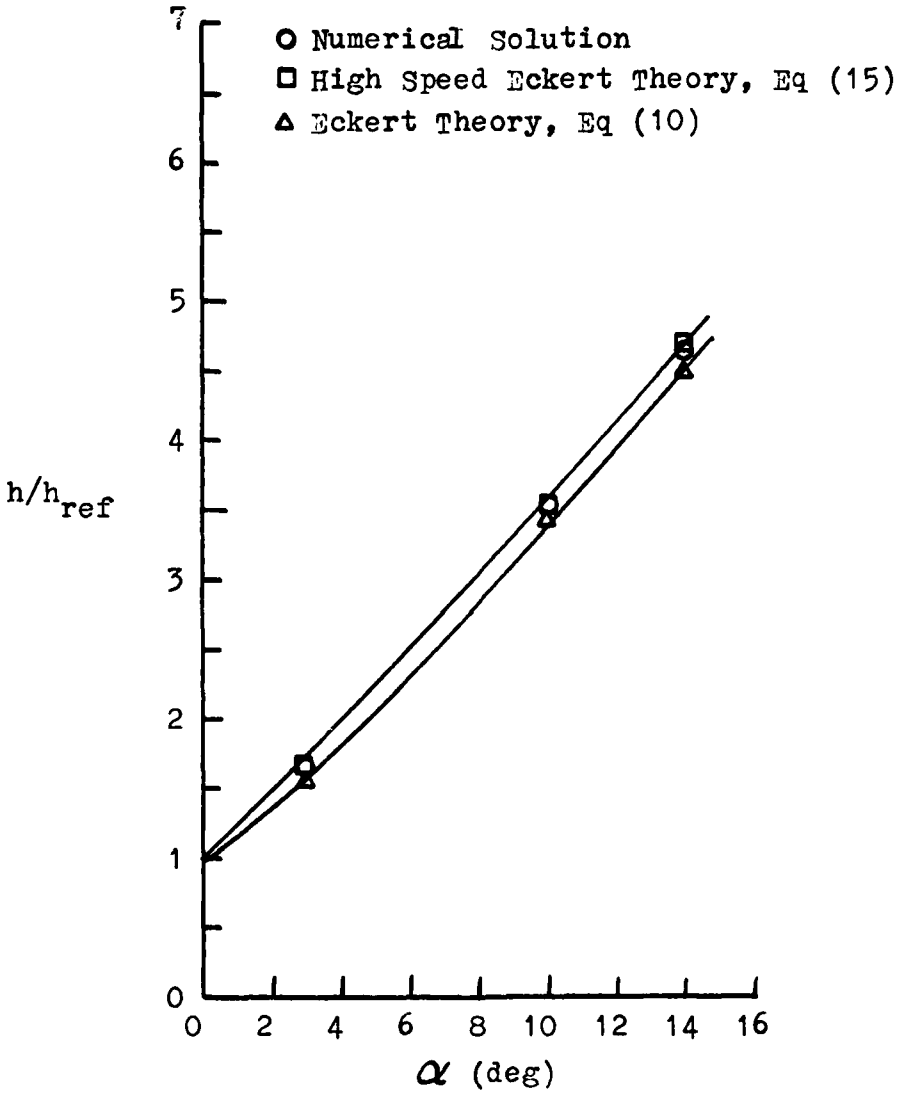

Figure 17. Comparison of Isothermal Wall, Low Temperature Heat Transfer Coefficient Calculations ($x/L = 0.575$)

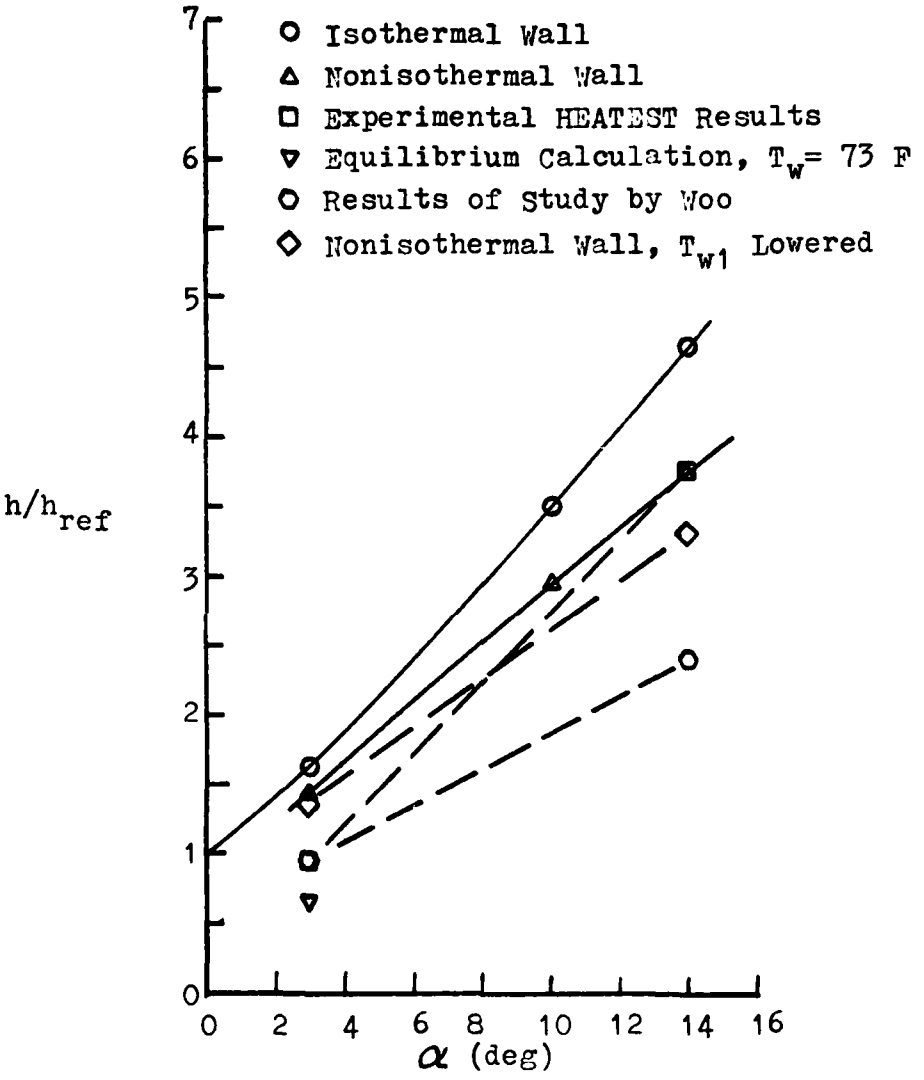

Figure 18. Comparison of Experimental, Isothermal, and Nonisothermal Heat Transfer Coefficient Calculations (x/L = 0.575)

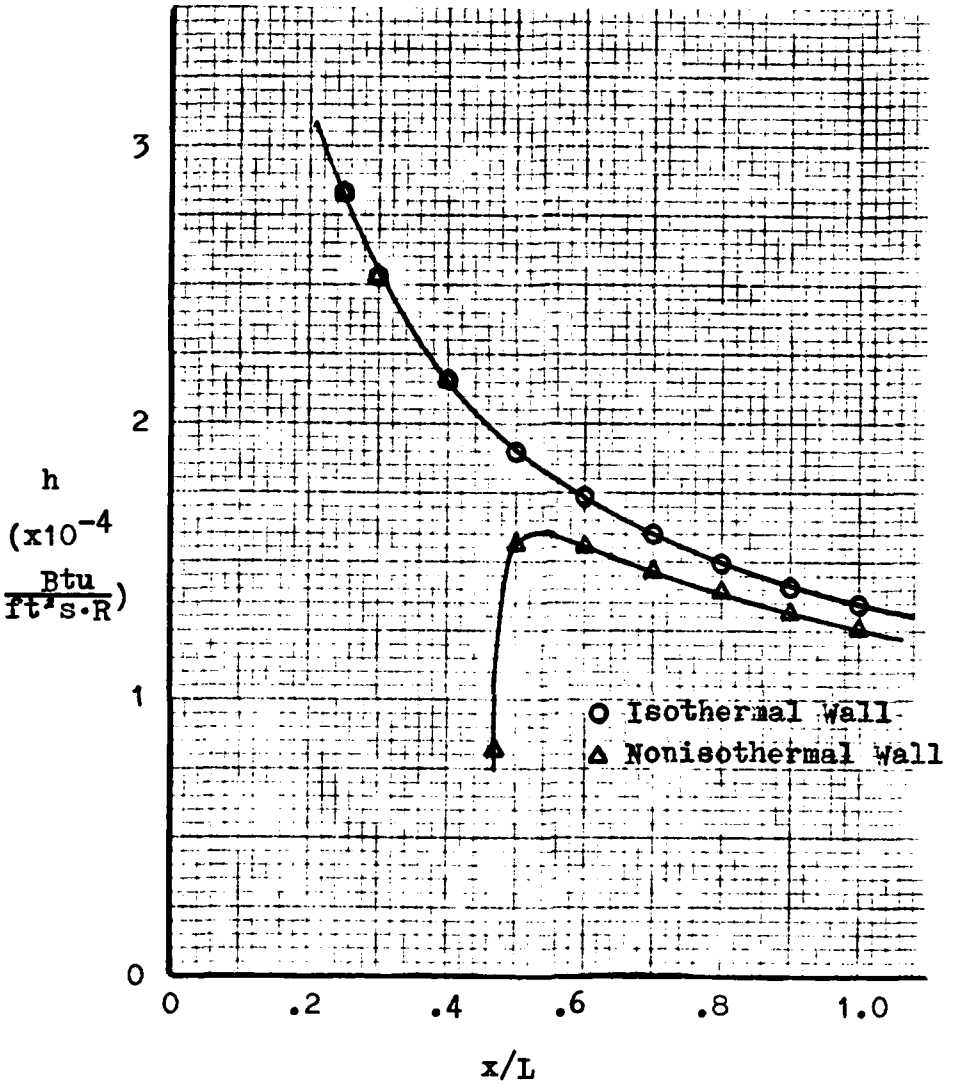

Figure 19. Streamwise Distribution of Heat Transfer Coefficient (α = 3 degrees)

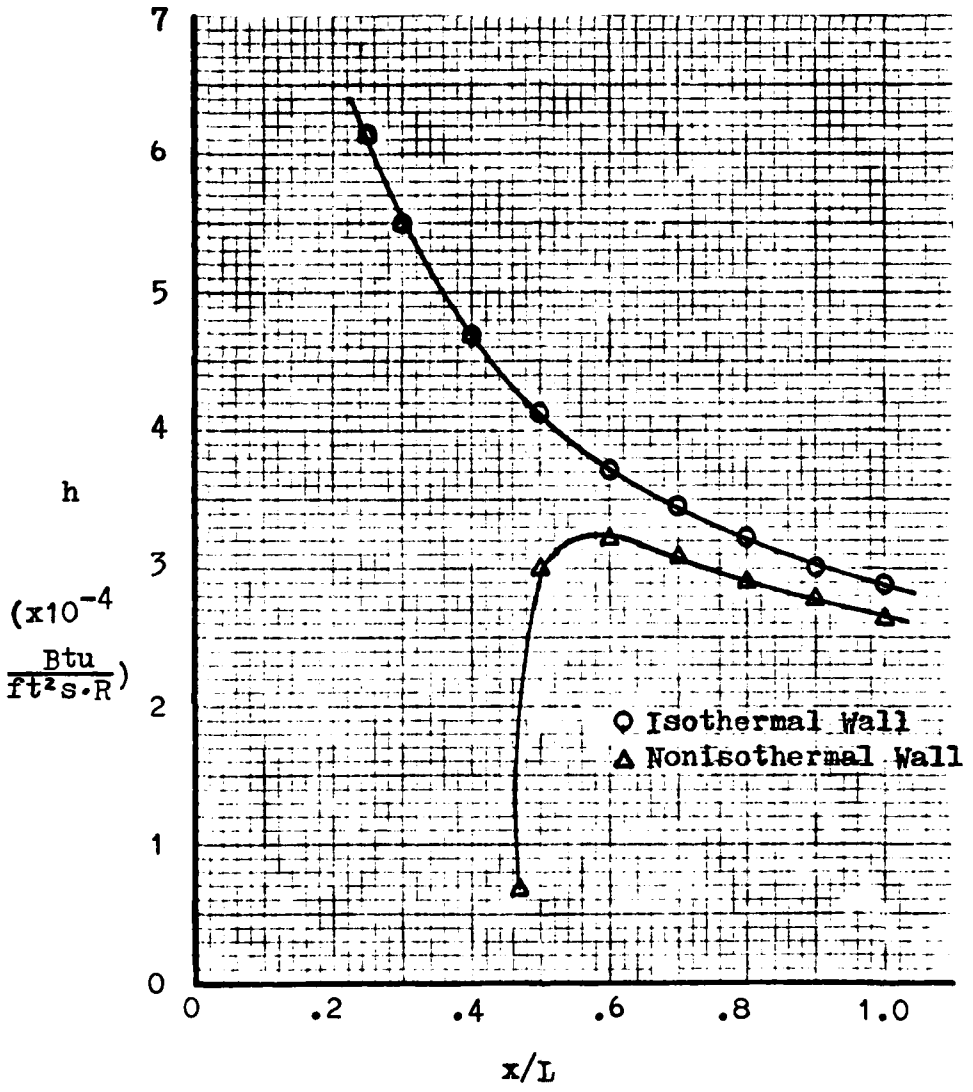

Figure 20. Streamwise Distribution of Heat Transfer Coefficient (α = 10 degrees)

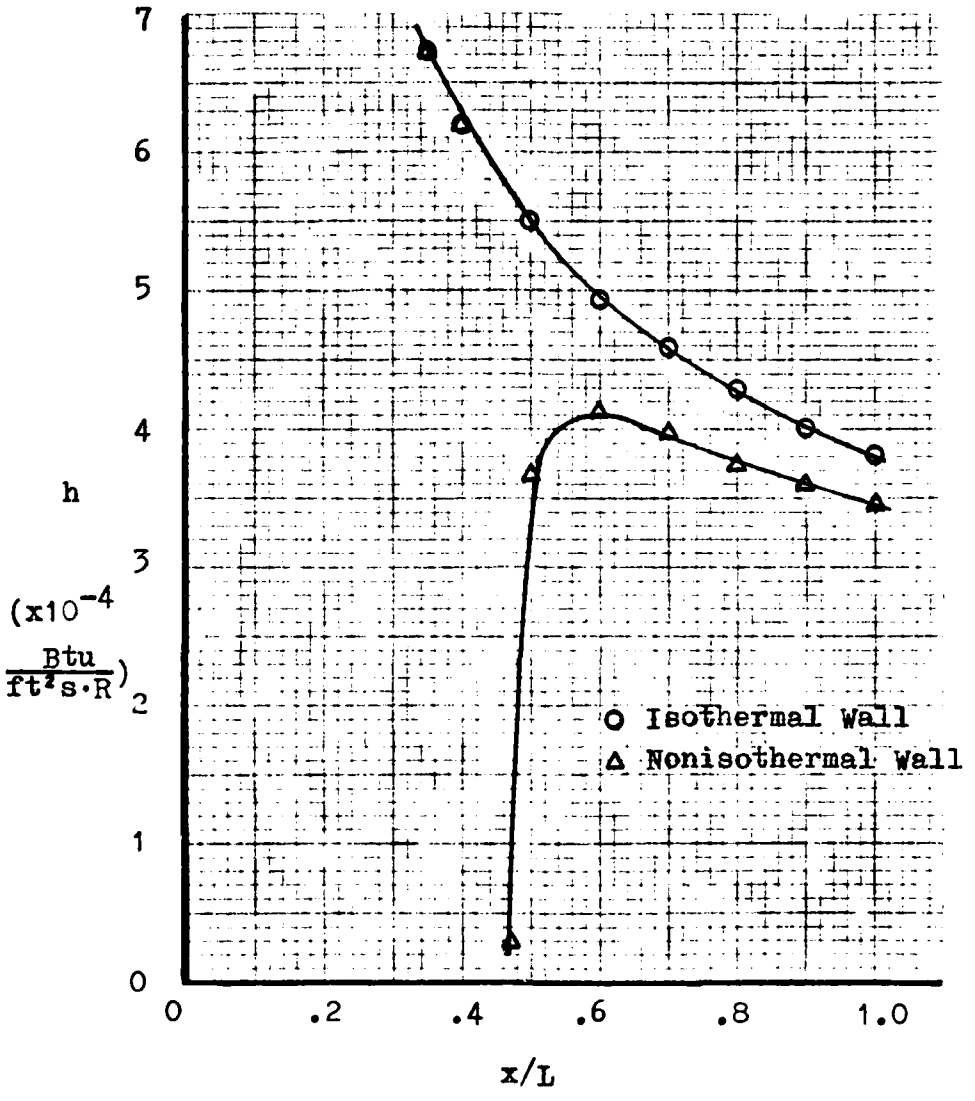

Figure 21. Streamwise Distribution of Heat Transfer Coefficient (α = 14 degrees)

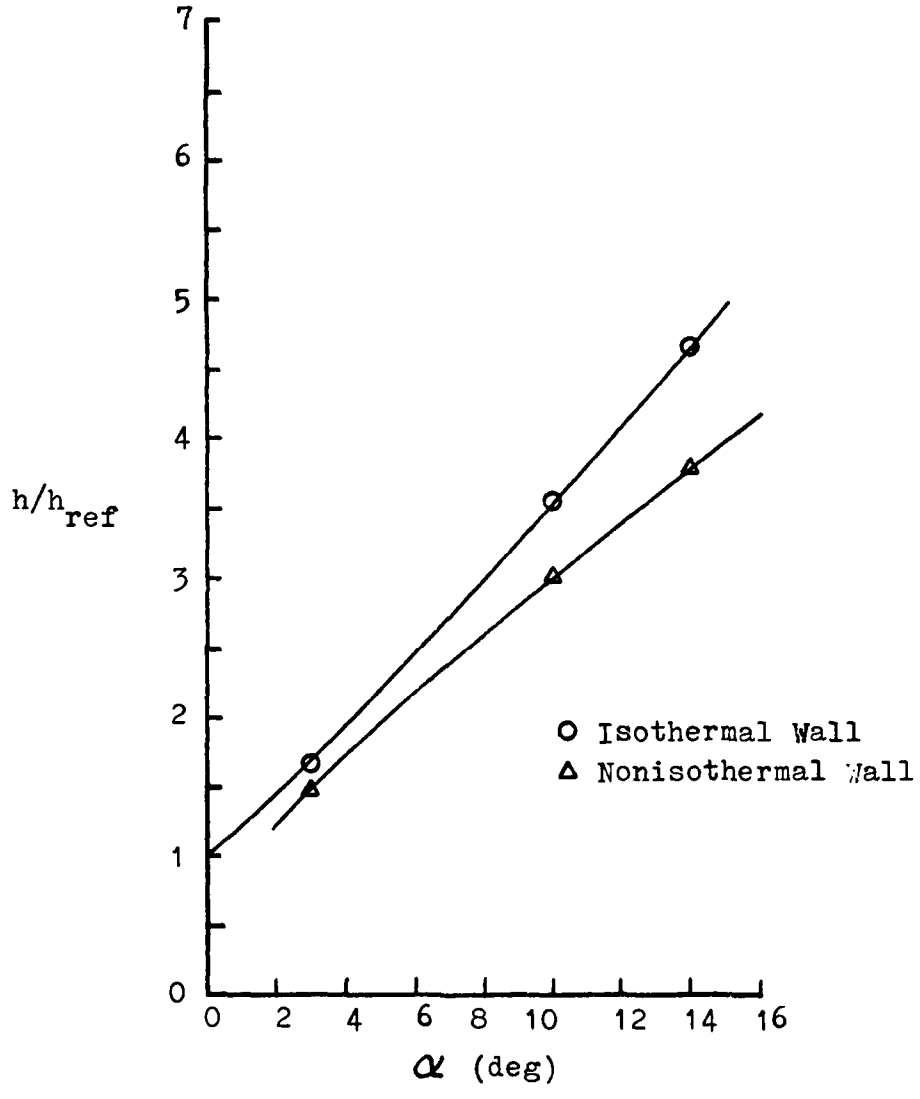

Figure 22. Comparison of Isothermal and Nonisothermal Heat Transfer Coefficient Calculations with Low Temperature Viscosity (x/L = 0.575)

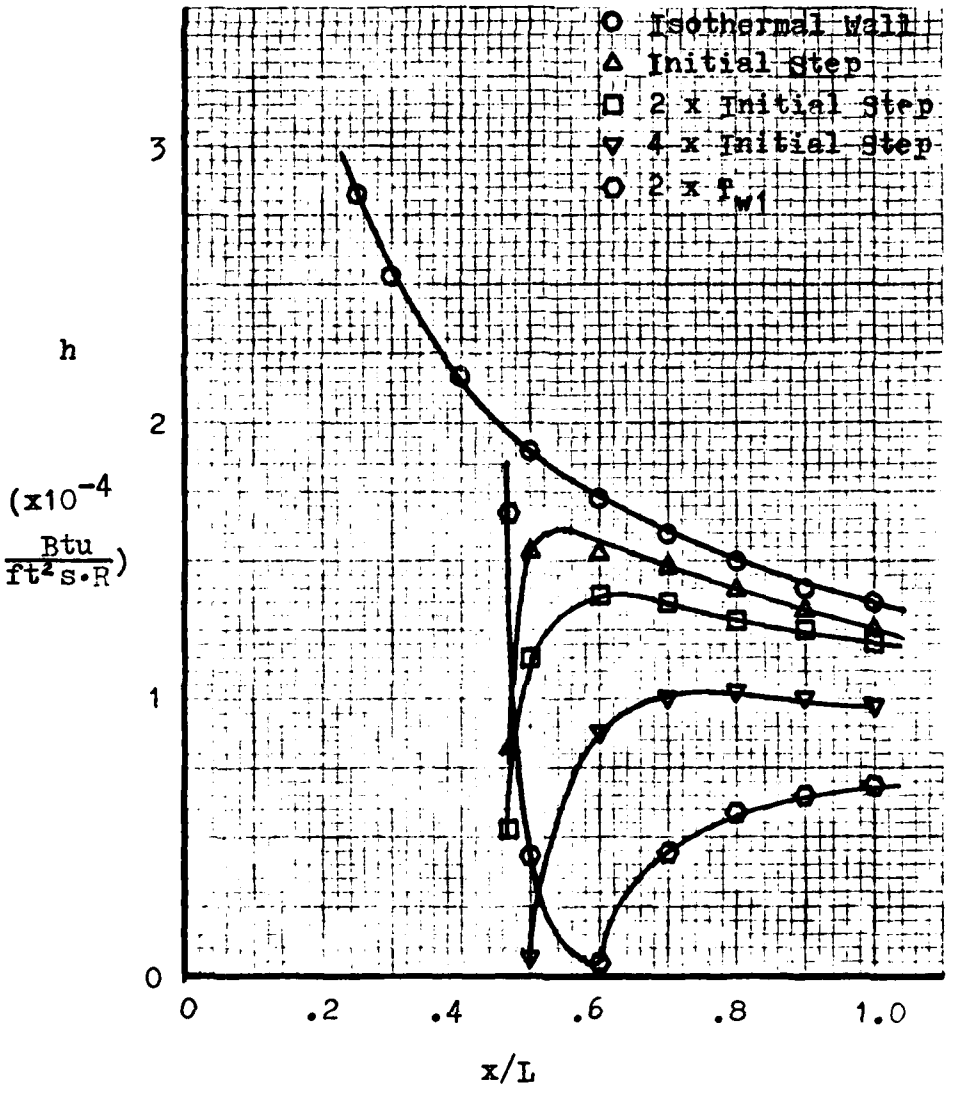

Figure 23. Streamwise Distribution of Heat Transfer Coefficient with Varying Step Size (α = 3 degrees)

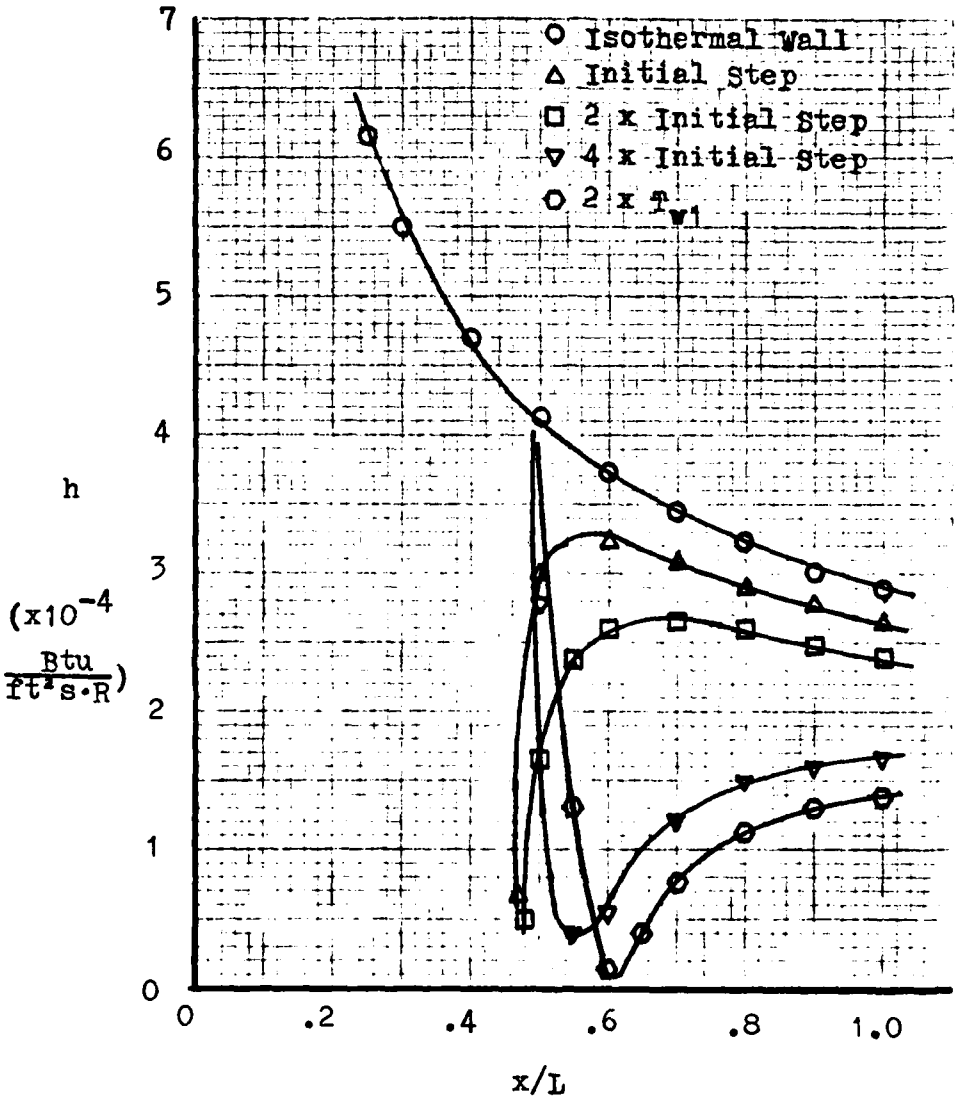

Figure 24. Streamwise Distribution of Heat Transfer Coefficient with Varying Step Size (α = 10 degrees)

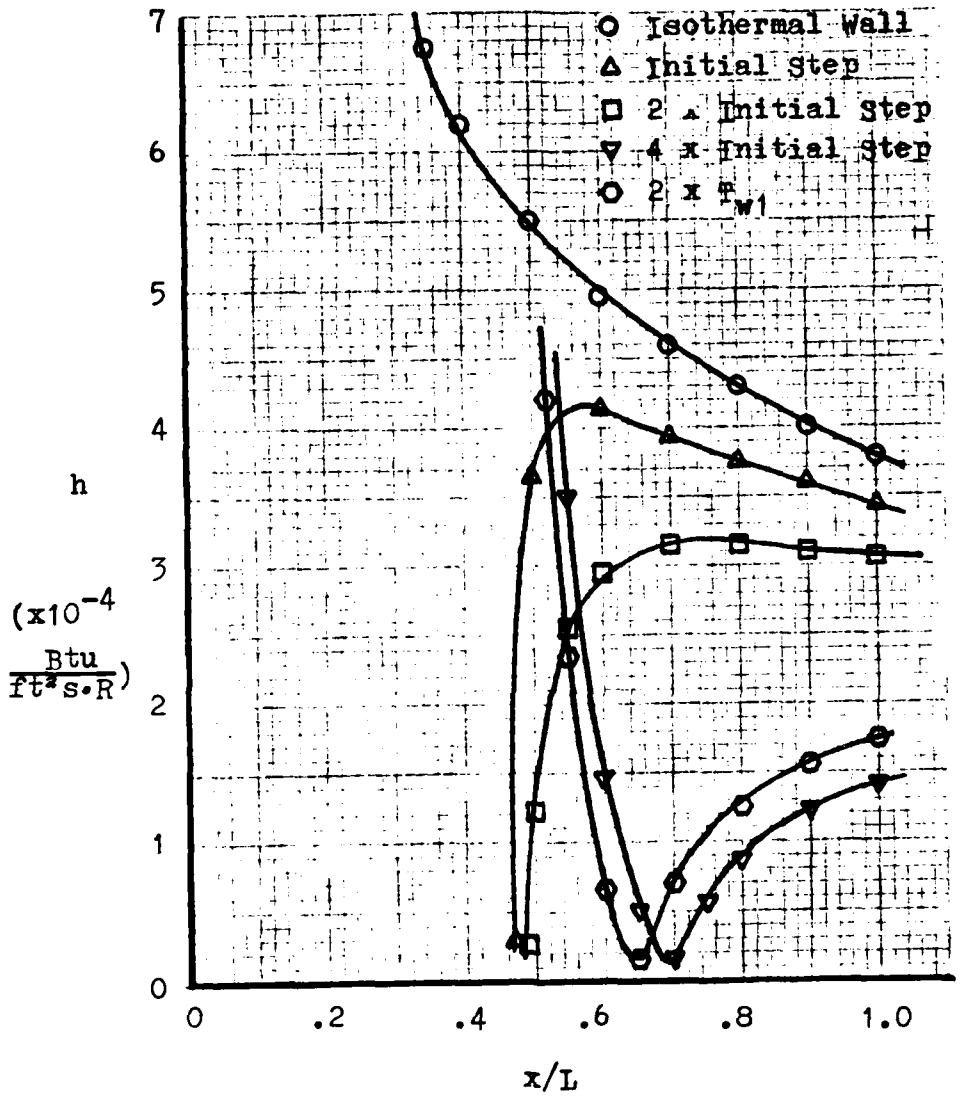

Figure 25. Streamwise Distribution of Heat Transfer Coefficient with Varying Step Size (α = 14 degrees)

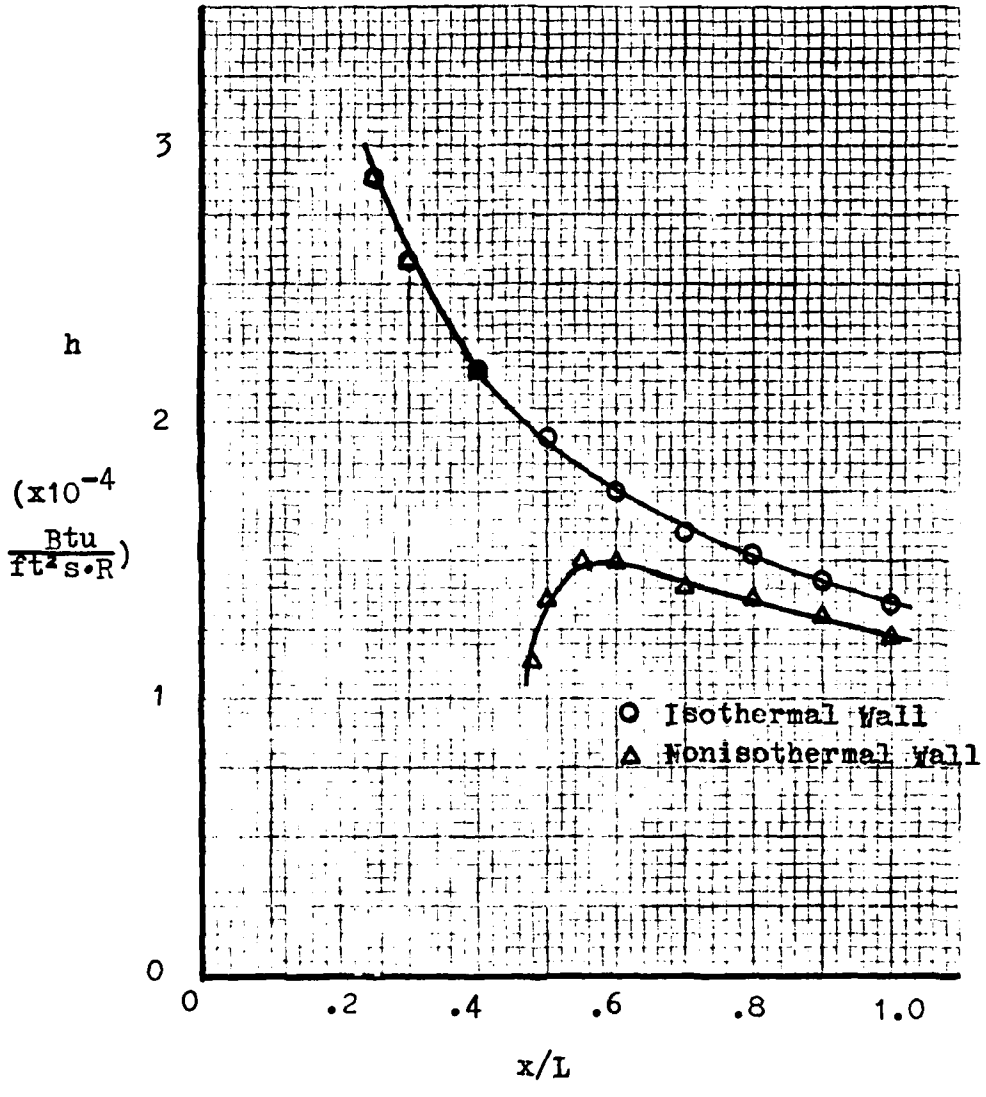

Figure 26. Streamwise Distribution of Heat Transfer Coefficient with Initial Wall Temperature Change (α = 3 degrees)

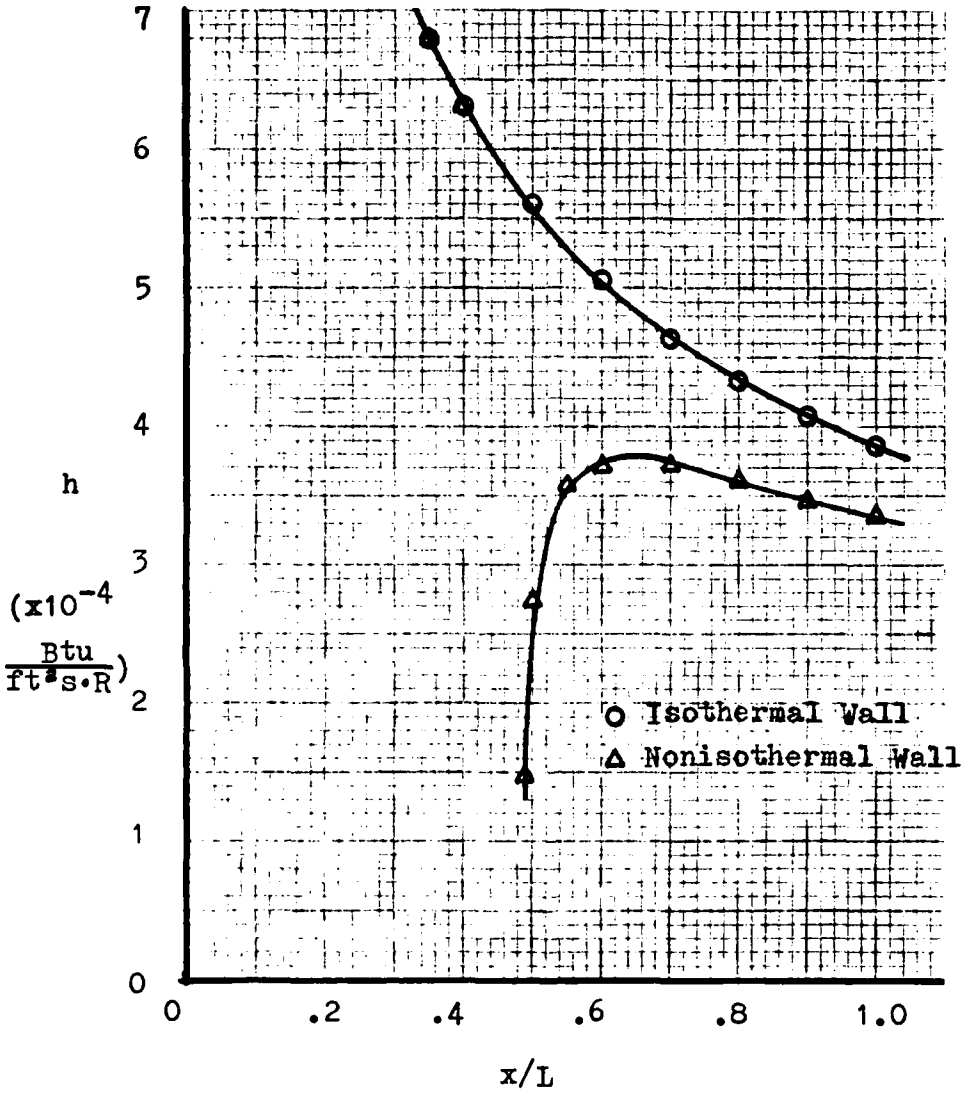

Figure 27. Streamwise Distribution of Heat Transfer Coefficient with Initial Wall Temperature Change (α = 14 degrees)

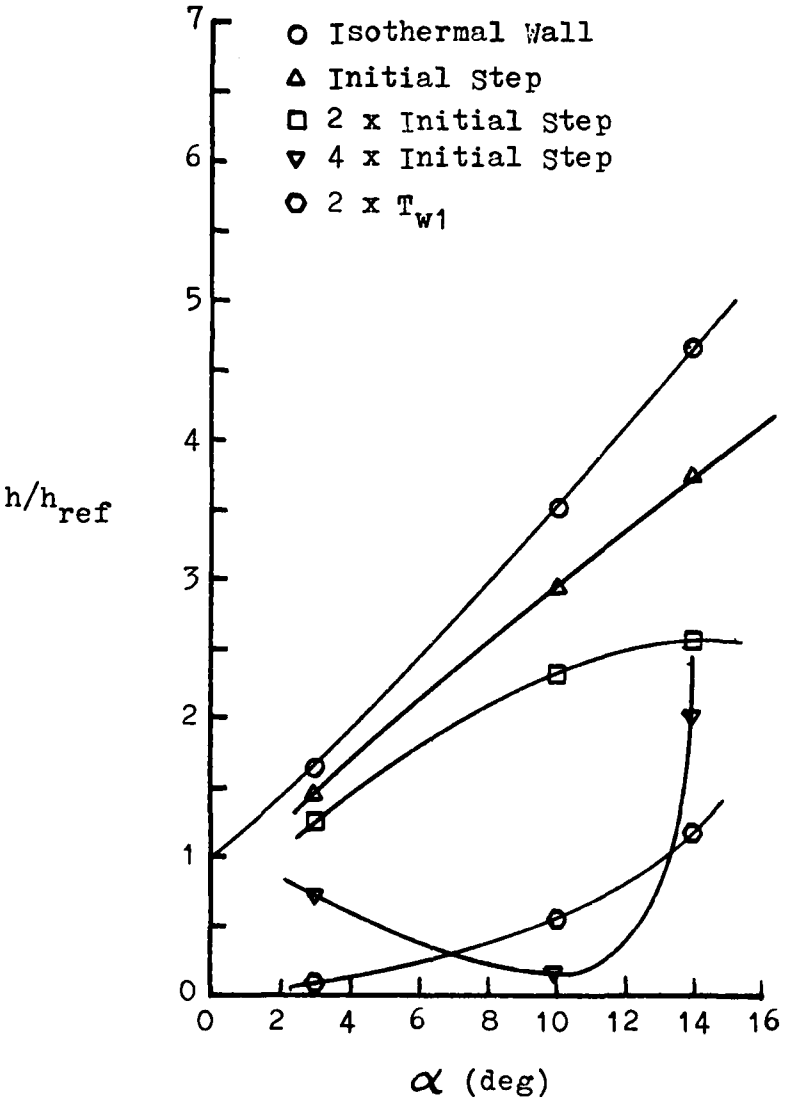

Figure 28. Comparison of Heat Transfer Coefficient with Varying Step Size (x/L = 0.575)

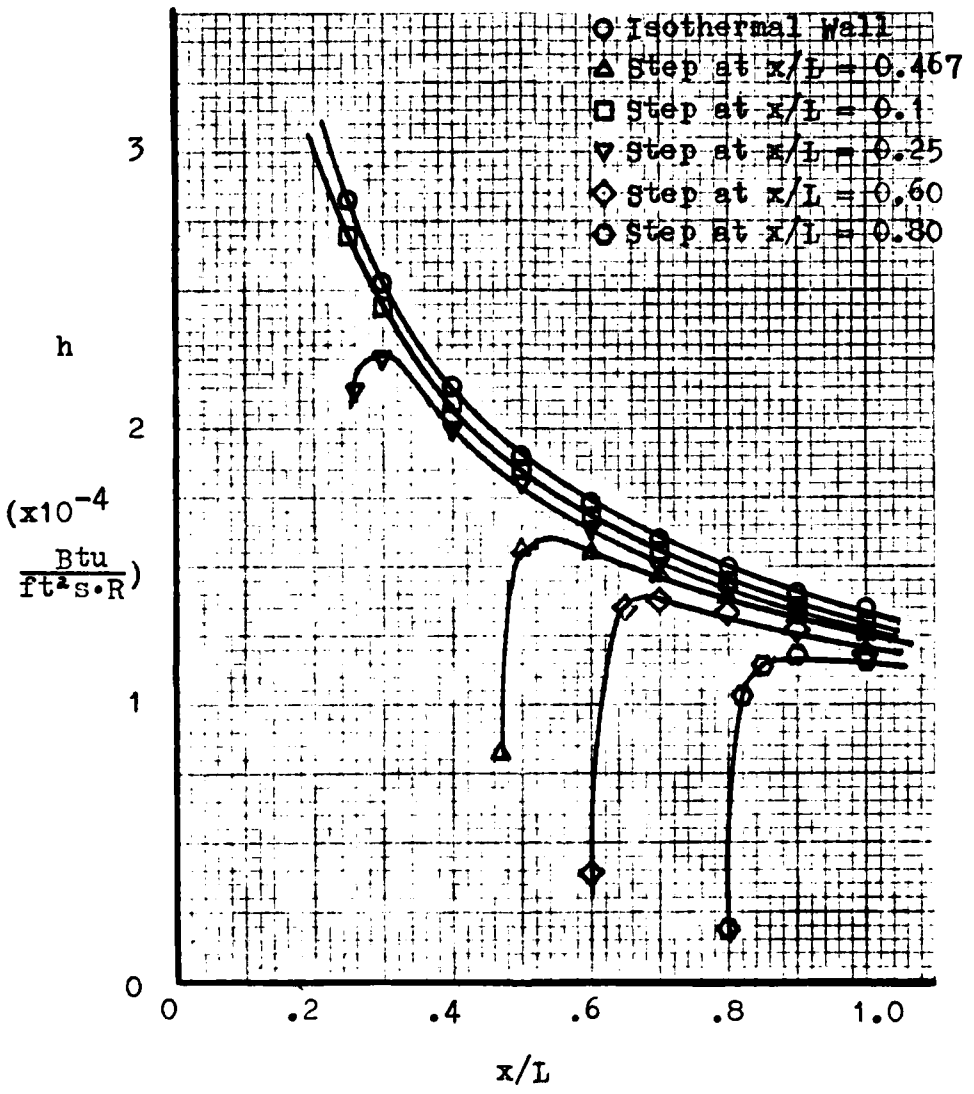

Figure 29. Comparison of Streamwise Distribution of Heat Transfer Coefficient with Varying Step Location (α = 3 degrees)

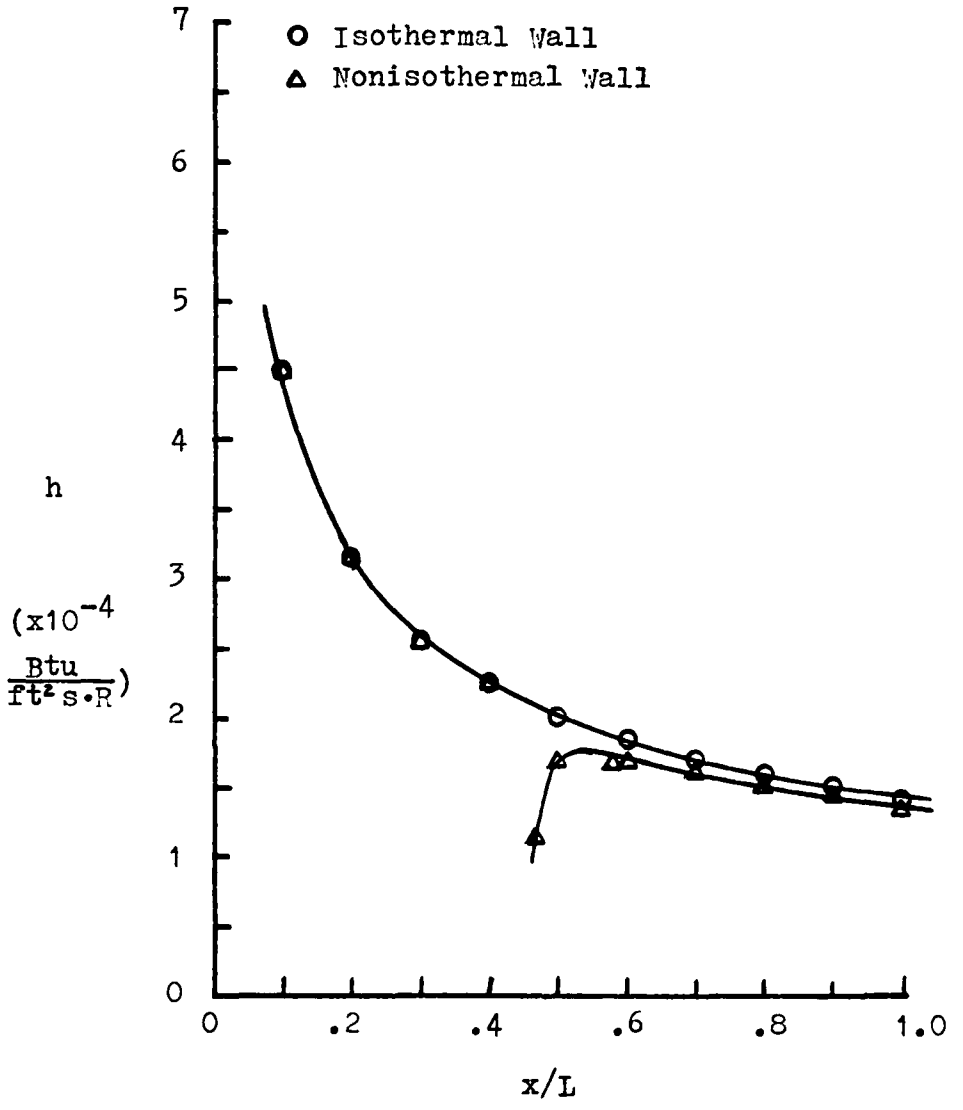

Figure 30. Streamwise Distribution of Heat Transfer Coefficient by Wall Temperature Superposition Analysis (α= 3 degrees)

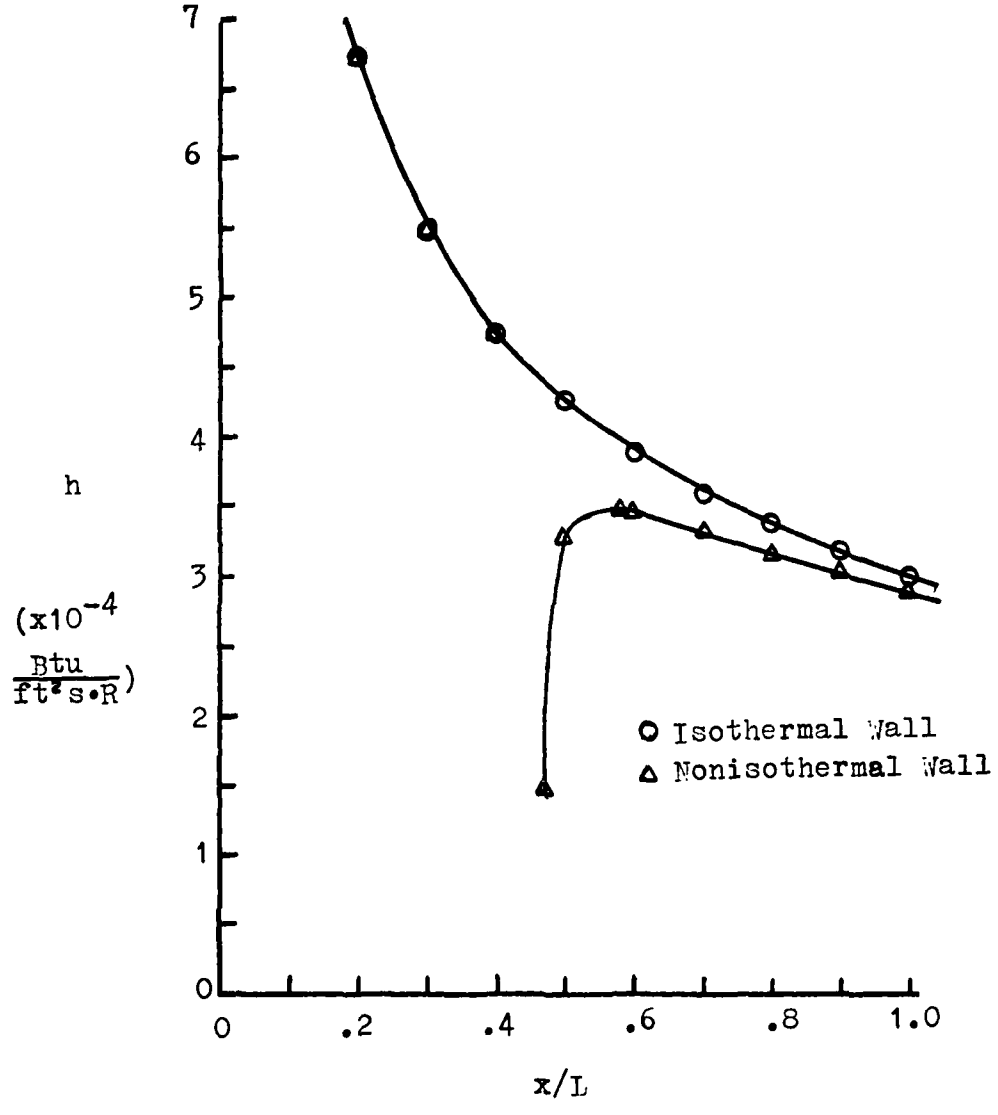

Figure 31. Streamwise Distribution of Heat Transfer Coefficient by Wall Temperature Superposition Analysis (α= 10 degrees)

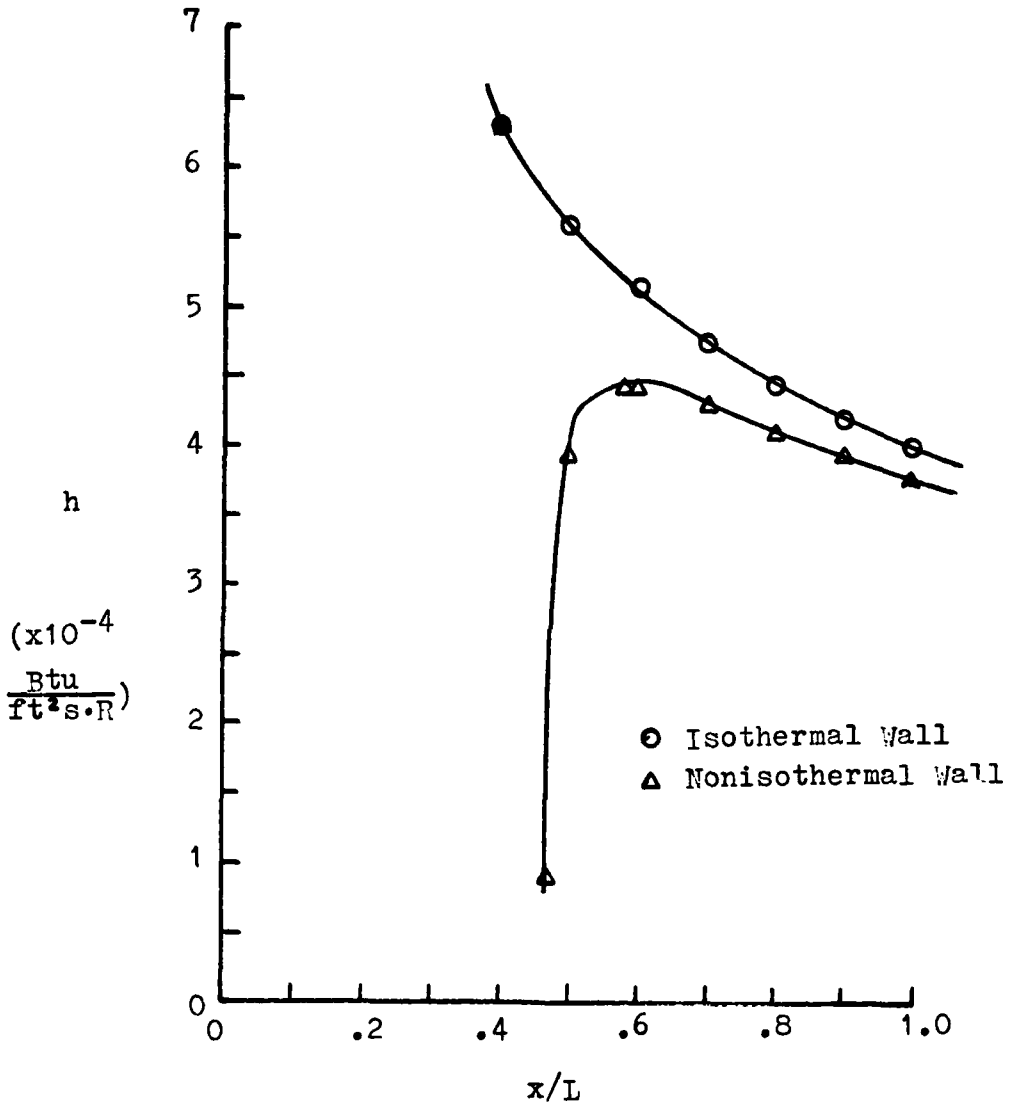

Figure 32. Streamwise Distribution of Heat Transfer Coefficient by Wall Temperature Superposition Analysis (α = 14 degrees)

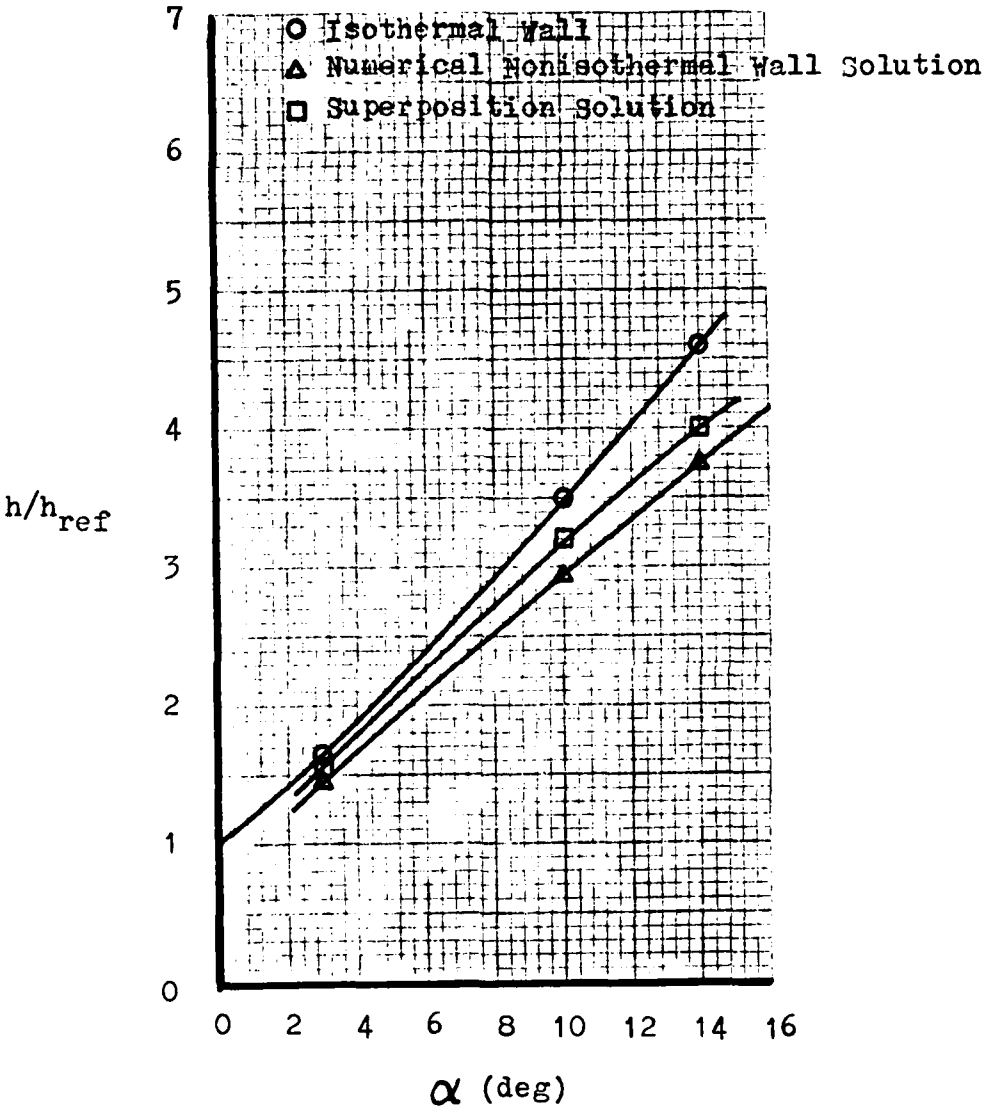

Figure 33. Comparison of Nonisothermal Wall Calculations of Heat Transfer Coefficient ($x/L = 0.575$)

Bibliography

1. Hodge, J. K., P. W. Phillips, and D. R. Audley. "Flight Testing a Manned Lifting Reentry Vehicle (Space Shuttle) for Aerothermodynamic Performance," AIAA Paper AIAA-81-2421, AIAA 1st Flight Testing Conference, November 1981.

2. Eckert, E. R. G. "Survey of Boundary Layer Heat Transfer at High Velocities and High Temperatures," WADC Technical Report 59-624, WADC, April 1960.

3. Hayes, J. R. and R. D. Neumann. "Trends in the Space Shuttle Aerothermodynamic Data Base," AIAA Paper AIAA-81-0292, AIAA 19th Aerospace Sciences Meeting, January 1981.

4. Kays, W. M. Convective Heat and Mass Transfer. New York: McGraw-Hill Book Company, 1966.

5. Fiore, A. W. "Viscosity of Air," Journal of Spacecraft and Rockets, 3 (5):756-758 (May 1966).

6. Keyes, F. G. "A Summary of Viscosity and Heat Conduction Data for He, A, H_2, N_2, CO, CO_2, H_2O, and Air," Transactions of ASME, 73:589-596 (1951).

7. Hayes, J. R. Data transmittal of magnetic tape and thin skin data from Shuttle test. Air Force Wright Aeronautical Laboratories, Wright-Patterson AFB, 13 April 1981.

8. Holman, J. P. Heat Transfer (Fifth edition). New York: McGraw-Hill Book Company, 1981.

9. Woo, Y. K. Transient Heat-Transfer Measurement Technique in Wind Tunnel and Data Analysis Technique Using System Identification Theory. MS Thesis. Wright-Patterson AFB, Ohio: Air Force Institute of Technology, December 1982.

10. Hankey, Wilbur. Lecture notes distributed in AE 6.30, Reentry Aerodynamics. School of Engineering, Air Force Institute of Technology, Wright-Patterson AFB, April 1982.

11. Cohen, C. B. and E. Reshotko. "Similar Solutions for the Compressible Laminar Boundary Layer with Heat Transfer and Pressure Gradient," NACA Report 1293, 1956.

12. Nachtsheim, P. R. and P. Swigert. "Satisfaction of Asymptotic Boundary Conditions in Numerical Solution of Systems of Nonlinear Equations of Boundary Layer Type," NASA Report TN D-3004, October 1965.

13. Beauregard, A. J. An Analytical Study of the Effects of Mass Transfer on a Compressible Turbulent Boundary Layer. MS Thesis. Wright-Patterson AFB, Ohio: Air Force Institute of Technology, December 1976.

Appendix A

Similarity Derivation and Applicability

Since much of the focus of this project was based on a model of the boundary layer flow, the application of similarity equations was a method worth consideration. No reference was found yielding the derivation of similarity equations for high speed flow with Prandtl Number unequal to unity. For future consideration, this derivation is included here, and will parallel the development used by Hankey (Ref 10).

Starting with the two-dimensional boundary layer equations,

$$(\rho u)_x + (\rho v)_y = 0 \tag{A-1}$$

$$\rho u u_x + \rho v u_y = (\mu u_y)_y + \rho_e u_e u_{e_x} \tag{A-2}$$

$$\rho u H_x + \rho v H_y = \mu[H_y]_y + [(1-Pr)kT_y]_y \tag{A-3}$$

and defining the stream function ψ such that $\rho u = \psi_y$ and $\rho v = -\psi_x$, the boundary layer equations may be written as

$$\psi_{xy} - \psi_{yx} = 0 \tag{A-4}$$

$$\psi_y u_x - \psi_x u_y = (\mu u_y)_y + \rho_e u_e u_{e_x} \tag{A-5}$$

$$\psi_y H_x + \psi_x H_y = [\mu H_y + (1 - Pr)kT_y]_y \tag{A-6}$$

where Eq (A-4) is identically satisfied as long as the stream function is continuous with respect to the independent vari-

AD-A124 803 HEAT TRANSFER/BOUNDARY LAYER INVESTIGATION OF HEATING 2/2
DISCREPANCIES IN WI..(U) AIR FORCE INST OF TECH
WRIGHT-PATTERSON AFB OH SCHOOL OF ENGI.. P T CAPPELANO
UNCLASSIFIED DEC 82 AFIT/GA/AA/82D-3 F/G 20/13 NL

END
DATE FILMED
83
DTIC

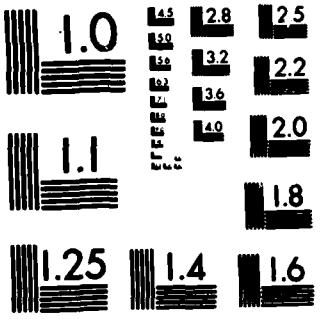

MICROCOPY RESOLUTION TEST CHART
NATIONAL BUREAU OF STANDARDS-1963-A

ables x and y. If the stream function is assumed separable with respect to the transformed variables ξ and η, it may be written as

$$\psi = g(\xi)\, f(\eta) \tag{A-7}$$

where $g = \sqrt{2\xi}$, and the transformed variables ξ and η are related to the independent variables x and y as

$$d\xi = j(x)dx \tag{A-8}$$

$$d\eta = h(x)\rho dy \tag{A-9}$$

with $j = \rho_e \mu_e u_e$ and $h = u_e/g$. By the chain rule, differentiation with respect to the variables x and y may now be defined as

$$\frac{\partial}{\partial x} = j \frac{\partial}{\partial \xi} + \eta_x \frac{\partial}{\partial \eta} \tag{A-10}$$

$$\frac{\partial}{\partial y} = h\rho \frac{\partial}{\partial \eta} \tag{A-11}$$

Making use of the above transformations and definitions, Eq (A-5) is reduced to

$$h\rho\rho_e u_e \mu_e (\psi_\eta u_\xi - \psi_\xi u_\eta) = h^2 \rho (\mu\rho u_\eta)_\eta + \rho_e^2 u_e^2 \mu_e u_{e\xi} \tag{A-12}$$

Defining $C = \frac{\mu\rho}{\mu_e \rho_e}$ allows further simplification to

$$h\rho u_e (\psi_\eta u_\xi - \psi_\xi u_\eta) = h^2 \rho (C u_\eta)_\eta + \rho_e u_e^2 u_{e\xi} \tag{A-13}$$

Dividing through by h^2 and reducing yields

$$(C u_\eta)_\eta = g(\psi_\eta u_\xi - \psi_\xi u_\eta) - \frac{\rho_e}{\rho} g^2 u_{e\xi} \tag{A-14}$$

Letting $f' = f_\eta = u/u_e$ and $S = (H/H_e) - 1$ gives

$$(Cf'')' = g\left[gf' \frac{u_\xi}{u_e} - f''\psi_\xi\right] - \frac{\rho_e}{\rho} g^2 \frac{u_{e\xi}}{u_e} \quad \text{(A-15)}$$

Further,

$$\frac{u_\xi}{u_e} = f' \frac{u_{e\xi}}{u_e} + f'_\xi = \frac{u}{u_e} \frac{u_{e\xi}}{u_e} + \frac{u_\xi}{u_e} - \frac{u}{u_e^2} u_{e\xi} \quad \text{(A-16)}$$

giving the final form

$$(Cf'')' + gf''\psi_\xi = g^2 \frac{u_{e\xi}}{u_e} (f'^2 - \frac{\rho_e}{\rho}) + g^2 f'f'_\xi \quad \text{(A-17)}$$

Similarly, the development of Eq (A-6) is found to yield

$$\psi_y H_x - \psi_x H_y = \left[\mu u u_y + \frac{\mu c_p}{Pr} T_y\right]_y \quad \text{(A-18)}$$

which, applying the transformation to variables ξ, η, gives

$$g\left[gf'H_\xi - \psi_\xi H_\eta\right] = \left[\frac{\rho\mu}{\rho_e\mu_e} (uu_\eta + \frac{c_p}{Pr} T_\eta)\right]_\eta \quad \text{(A-19)}$$

With the definition for S, the total enthalpy H may be used to transform the temperature T:

$$H = (S + 1)H_e \quad \text{(A-20)}$$

$$T = \frac{H - u^2/2}{c_p} \quad \text{(A-21)}$$

$$T_\eta = \frac{1}{c_p} (H_\eta - uu_\eta) \quad \text{(A-22)}$$

Differentiating the total enthalpy and velocity as

$$H_\eta = H_e S' \quad \text{(A-23)}$$

$$H_\xi = H_{e\xi}(S + 1) + H_e S_\xi \quad \text{(A-24)}$$

$$u_\eta = u_e f'' \tag{A-25}$$

These values can be substituted into Eq (A-19) to give

$$g^2 f' \left[H_{e\xi}(S + 1) + H_e S_\xi\right] - g H_e S' \psi_\xi =$$

$$\left[\frac{\rho\mu}{\rho_e \mu_e}\left(f' f'' u_e^2 \left(\frac{Pr - 1}{Pr}\right) + \frac{1}{Pr} H_e S'\right)\right]_\eta \tag{A-26}$$

Again using the definition of $C = \frac{\rho\mu}{\rho_e \mu_e}$ and realizing that total enthalpy is constant, Eq (A-26) becomes

$$(CS')_\eta + Pr g S' \psi_\xi = Pr\left[g^2 f' S_\xi - \frac{u_e^2}{H_e}\left(\frac{Pr-1}{Pr}\right)(Cf'f'')_\eta\right] \tag{A-27}$$

Applying the similarity conditions that the value C is constant and equal to unity and that the functions f and S are independent of streamwise location, (i.e. $S_\xi = 0$, $\psi_\xi = f/g$), Eqs (A-17) and (A-27) are further reduced to

$$f''' + ff'' = \beta(f'^2 - S - 1) \tag{A-28}$$

$$S'' + Prf S' = (1 - Pr)\left[\frac{(\gamma-1)M_e^2}{1+\frac{\gamma-1}{2}M_e^2}\right](f' f''' + f''^2) \tag{A-29}$$

where $\beta = g^2 \frac{H_e u_{e\xi}}{h_e u_e} = 2\xi \frac{M_{e\xi}}{M_e}$ and $f'^2 - \frac{\rho_e}{\rho} = \frac{H_e}{h_e}(f'^2 - S - 1)$. Note that these expressions agree with those given by Cohen and Reshotko (Ref 11). These equations are valid so long as the similarity conditions are met.

For the conditions of the wind tunnel tests run, the insulating articles used were assumed to be at thermal equilibrium between boundary layer heating and radiation. For radiation

$$q = \epsilon\sigma T_w^4 \tag{A-30}$$

assuming zero sink temperature. The heating of the wall is given as

$$q = -k \left.\frac{\partial T}{\partial y}\right|_{y=0} \tag{A-31}$$

At the wall, velocity is zero and $H = c_p T$ or $T = H/c_p$. Substituting and equating the above expressions yields

$$\left[\frac{k}{c_p}\frac{\partial H}{\partial y} = -\epsilon\sigma\left(\frac{H}{c_p}\right)^4\right]_{y=0} \tag{A-32}$$

Defining the function S as before and using the differentiation of Eqs (A-10) and (A-11), the equilibrium condition is expressed as

$$\left[S' = \frac{\epsilon\sigma H_e^4 g}{k u_e \rho_e T_e c_p^4}\,(S+1)^5\right]_{\eta=0} \tag{A-33}$$

In this form, g is a function of the streamwise location denoted by ξ. As a result, the function S is no longer independent of ξ, as necessary by the similarity assumptions. In this case similarity is no longer valid, and must be discarded as a solution technique.

For those cases where similarity is valid, solution of the given equations may be accomplished according to the technique given by Nachtsheim and Swigert (Ref 12).

Appendix B

Numerical Computation

All numerical calculations were accomplished using the boundary layer program alluded to earlier. Access to this program was gained from Mr. George Havener. The program used was identical to that found in Ref 13 given the folowing modifications:

1) omit lines 200-220,
2) omit line 260,
3) substitute for line 420 with

```
READ (5,8002) G, PR, XMINF, REY, TA
```

4) omit lines 480-610,
5) omit lines 5120-5130,
6) omit lines 5260-5310,
7) substitute between lines 5250 and 5320 with

```
D3(1) = 0.
```

8) substitute between lines 7480 and 7490 with

```
TTR = (TA + 112.)/(TA*TREF + 112.)
```

9) omit lines 7990 and 8020,
10) substitute between lines 7980 and 8030 with

```
EP(N) = EP(N)*(1.-EXP(-.412*((S-BTRX)/XLAM)**2.))
```

11) omit lines 11950-12450.

The program itself, called ITRACT, computes boundary layer flow characteristics for laminar and/or turbulent boundary layers, over flat plates or axisymmetric bodies. The computation was accomplished through transformation of the non-linear parabolic boundary layer equations into a rectangular grid, and subsequent solution of this system of equations by linear finite differencing, using a three-point scheme

with a tridiagonal matrix inversion routine. The solution of the boundary layer was thus calculated at incremental streamwise locations. A complete discussion of the technique used in this boundary layer program is given by Beauregard (Ref 13).

The characteristics input to the program itself included the specific heat ratio γ, Prandtl Number Pr, boundary layer edge Mach Number M_e, edge temperature T_e, edge Reynolds Number based on total plate length R_{e2}, as well as wall temperature to stagnation temperature ratio, flow transition location, viscosity law selection parameter, and calculation parameters. The specific heat ratio and Prandtl Number were assumed constant for all cases at $\gamma = 1.4$ and $Pr = 0.72$. Boundary layer edge properties of Mach Number, static temperature, and Reynolds Number were input appropriately for the case considered. Wall temperature to stagnation temperature ratio was derived from the wall temperature given by thin skin data, assuming a stagnation temperature of $T_o = 2000$ R for all cases. Sutherland's Law for viscosity was used in all cases, except as discussed in consideration of the alternate low temperature viscosity relationship. The flow transition location was arbitrarily chosen as unity (end of the plate) since flow was assumed to be laminar in all cases. This assumption was made for several reasons. No indication of transition over the test apparatus was found, and no location for transition could be given. The freestream Reynolds Number was found to be approximately one million, with the location of interest

at approximately one half the plate length giving a Reynolds Number locally of roughly one-half million. In addition, much care was taken in installing the test articles to prevent a boundary layer trip. Since heating data for the test runs made give relatively smooth, continuous heating, no transition is indicated. Lastly, experience with the wind tunnel used indicates that turbulent flow is unlikely and difficult to attain at operational conditions.

Output data included boundary layer velocity profile, thickness, momentum thickness, displacement thickness, local Reynolds Number, and local Stanton Number. From the local Stanton Number, the local heat transfer coefficient was derived.

In order to estimate the effect of the wall temperature step on the heat transfer coefficient, the program had to be modified to accommodate a step change in the wall to stagnation temperature ratio. This modification was accomplished by inserting the following lines between lines 1480 and 1500 in the program listed in Ref 12:

```
      IF (S. LT . 0.467) GO TO 500
      BO = .3500
      T1 = BO * T10
  500 DX2DS = DX1DS
```

The value of the wall to stagnation temperature ratio, denoted BO above, is based on the total wall temperature following the step, given by the HRSI test data cited. This value varies depending on the stagnation temperature and final wall temperature desired.

Estimation of boundary layer characteristics based on the low temperature viscosity calculation required some additional modification of the program. The following changes account for the alternate viscosity relationship:

1) omit line 880,
2) substitute the following lines between lines 870 and 890:

```
SU = 220./10.**(9./TA)
TR = SU/TA
TREF = (G-1.)*XMINF**2.
TC = TR/TREF
```

3) substitute the following for lines 900 to 910:

```
EPS = (((1.+TR)*TREF**1.5)/((TREF+TR)*REY))**0.5
```

4) substitute for line 930 with

```
102 CONTINUE
```

5) omit line 1630,
6) substitute for line 1670 with

```
676 XNUE = VISINF
```

7) omit line 1300.

Note that the modifications for the low temperature viscosity calculation assume that this method is replacing the Sutherland's Law calculation and replaces statements accordingly. The same viscosity calculation parameter is used in the input data. Laminar flow is also assumed, and additional changes may be required for turbulent flow applications.

Lastly, a check was made for numerical solution inaccuracy due to increment size. This check was made for the nonisothermal case of α = 3 degrees . The increment size, originally set at Δx = 0.0001 , was doubled to Δx = 0.0002 , and halved to Δx = 0.00005 to verify accuracy. The result

for this check showed an error of five percent above the value used both before the step and at the HRSI thermocouple location for the increment $\Delta x = 0.0002$. When the increment was halved, or $\Delta x = 0.00005$, an error of two percent below the calculated value was found between this and the original case of $\Delta x = 0.0001$, for both locations, before and after the wall temperature step. It would appear that accuracy was still increasing with decreasing increment size at the values used.

Vita

Peter T. Cappelano was born on 26 August 1959 in Couvron, Aisne, France. He graduated from Mount Saint Charles Academy, Woonsocket, Rhode Island in 1977 and attended the University of Notre Dame, from which he received the degree of Bachelor of Science in Aerospace Engineering in May 1981. Upon graduation, he received a commission in the USAF through the ROTC program, and entered the School of Engineering, Air Force Institute of Technology, in June 1981.

Permanent address: 85 Temi Rd
Bellingham, Massachusetts 02019

SECURITY CLASSIFICATION OF THIS PAGE (When Data Entered)

REPORT DOCUMENTATION PAGE		READ INSTRUCTIONS BEFORE COMPLETING FORM
1. REPORT NUMBER AFIT/GA/AA/82D-3	2. GOVT ACCESSION NO. AD-A124 803	3. RECIPIENT'S CATALOG NUMBER
4. TITLE (and Subtitle) HEAT TRANSFER/BOUNDARY LAYER INVESTIGATION OF HEATING DISCREPANCIES IN WIND TUNNEL TESTING OF ORBITER INSULATING ARTICLES		5. TYPE OF REPORT & PERIOD COVERED MS Thesis 6. PERFORMING ORG. REPORT NUMBER
7. AUTHOR(s) Peter T. Cappelano		8. CONTRACT OR GRANT NUMBER(s)
9. PERFORMING ORGANIZATION NAME AND ADDRESS Air Force Institute of Technology (AFIT-EN) Wright-Patterson AFB, Ohio 45433		10. PROGRAM ELEMENT, PROJECT, TASK AREA & WORK UNIT NUMBERS
11. CONTROLLING OFFICE NAME AND ADDRESS		12. REPORT DATE December, 1982 13. NUMBER OF PAGES 106
14. MONITORING AGENCY NAME & ADDRESS(if different from Controlling Office)		15. SECURITY CLASS. (of this report) Unclassified 15a. DECLASSIFICATION/DOWNGRADING SCHEDULE

16. DISTRIBUTION STATEMENT (of this Report)

Approved for public release; distribution unlimited

17. DISTRIBUTION STATEMENT (of the abstract entered in Block 20, if different from Report)

18. SUPPLEMENTARY NOTES

Approved for public release; IAW AFR 190-17

LYNN E. WOLAVER
Dean for Research and Professional Development
Air Force Institute of Technology (ATC)
Wright-Patterson AFB OH 45433

4 JAN 1983

19. KEY WORDS (Continue on reverse side if necessary and identify by block number)

Nonisothermal wall
Orbiter Insulating Articles
Heat Transfer
Boundary Layer
Low temperature viscosity
Wall Temperature Superposition
Eckert high speed theory

20. ABSTRACT (Continue on reverse side if necessary and identify by block number)

Wind tunnel test runs were conducted on Space Shuttle orbiter insulating articles. The data from one HRSI run was processed by a heat estimation program, revealing a large discrepancy in magnitude of the heat transfer coefficient over the HRSI tile when compared to that yielded by flat plate theory and thin skin results. An initial suggestion for the cause of this discrepancy was the nonisothermal wall effect. This effect was the subject of this investigation. The boundary layer heat transfer coefficient was evaluated

DD FORM 1 JAN 73 1473 EDITION OF 1 NOV 65 IS OBSOLETE

SECURITY CLASSIFICATION OF THIS PAGE (When Data Entered)

(from Item 20) using a numerical boundary layer program, supplemented by wall temperature superposition analysis. The program was shown to give results consistent with Eckert high speed, flat plate theory for the isothermal wall. A comparison of Sutherland's Law and a low temperature viscosity calculation showed little difference for the high speed flow. Theory based on reference temperature supported this result. The program was modified for wall temperature step over the insulating article to model heat transfer coefficient dependence on wall temperature variation. The step size was varied by doubling and quadrupling the initial step size, and by doubling the initial wall temperature. The magnitude of the heat transfer coefficient decreased, and response slowed, with increasing step size. The step location was also varied. Analysis by wall temperature superposition yielded results similar to program results with the initial wall temperature step. The nonisothermal wall effect appears to account for most of the discrepancy in the original wind tunnel test results.